Engineered Science
DOI: https://dx.doi.org/10.30919/es1565

Multi-Agent System of Car-Like Manipulators for Construction Operations in Dynamic Environments

Ravinesh Chand,[1, 2,*] Bibhya Sharma,[1] Dietmar Oelz[3] and Sandeep A. Kumar[1]

Abstract

The construction industry faces critical challenges today, including labour shortages, worker safety concerns and project delays. Adopting robotic automation, particularly in dynamic settings, has emerged as a viable solution to addressing these issues. This paper presents a new multi-agent system of four-arm car-like mobile manipulators designed to address these issues by automating labour-intensive tasks, enhancing safety and boosting productivity. Each manipulator combines the functionality of robotic arms with the mobility of an autonomous car-like vehicle, ensuring the homogeneous system can perform a range of tasks from material handling to complex assembly operations autonomously in dynamic environments. The core innovation of this research is the design of continuous acceleration-based controllers for these mobile manipulators using the Lyapunov-based control scheme (LbCS), which is a new application for a multi-agent system of four-arm car-like robots, providing a means to achieve higher levels of flexibility. The effectiveness of these controllers and the overall system performance have been validated through computer simulations, demonstrating the system's capability for executing complex tasks within a multi-agent network. This study lays the groundwork for transformative advancements in the construction industry through multi-agent robotic automation, with implications for enhanced operational efficiency and worker safety while providing a promising solution for addressing shortages in labour-intensive sectors.

Keywords: Multi-agent system; Construction robots; Mobile manipulators; Motion control; Collision-free navigation; Labour shortages.

Received: 01 December 2024; Revised: 08 May 2025; Accepted: 12 May 2025.
Article type: Research article.

1. Introduction

The construction industry is amongst those that contribute significantly to countries' economic development, with a 9% gross domestic product share and about 7-8.5% of total employment worldwide.[1-3] Traditionally renowned as being labour-intensive, the construction industry relies heavily on the manual operation of human workers to build new infrastructure and conduct renovations and demolitions. Today, the industry faces serious challenges such as environmental concerns, worker safety issues, project timeline delays, labour shortages and an ageing workforce due to the young generation being attracted to other industries, lured by rapid career progression, job stability and appealing work conditions.[3] The integration of advanced technologies, particularly within the framework of Industry 4.0, offers solutions to these challenges by automating labour-intensive tasks, improving worker safety and increasing productivity while attracting younger generations through the use of autonomous systems and innovative work environments. Intelligence digital tools such as big data, artificial intelligence (AI), machine learning (ML), robotics, and automation in industrial operations are crucial to enhance these benefits further.

Adopting robotic automation in construction settings has increased the demand for advanced automated navigation systems capable of operating in dynamic environments safely and efficiently. Robots are increasingly capable of performing repetitive and hazardous tasks consistently, minimizing

[1] *School of Information Technology, Engineering, Mathematics & Physics, The University of the South Pacific, Suva, 1168, Fiji*
[2] *School of Mathematical & Computing Sciences, Fiji National University, Suva, 1672, Fiji*
[3] *School of Mathematics and Physics, The University of Queensland, Brisbane, 4072, Australia*
**Email:* ravinesh.c@fnu.ac.fj (R. Chand)

accidents and reducing the need for manual labour. Recent studies depict that the construction industry is gradually embedding various types of mobile manipulators, including robotic arms on wheeled bases, which play a crucial role in increasing flexibility by expanding the range of tasks that can be completed autonomously.[1,4,5] Among the diverse range of robotic platforms, a mobile manipulator stands out for its versatility in complex manipulation tasks since the robotic arms significantly increase the workspace of the manipulators while navigating cluttered workspaces and, therefore, enable industries to achieve higher levels of productivity and flexibility.[1,6]

A mobile manipulator is a mechanical system that combines the mobility of a mobile base with the functionality of its robotic arms, offering the potential to accomplish repetitive tasks simultaneously. Depending on the specific application, mobile manipulators usually vary in the number of robotic arms installed, with robots equipped with single or dual arms being the common types of mobile manipulators that are researched and used in applications. [6-8] Considering the unique nature of construction projects, these systems may not be ideal for meeting the demands and requirements for accomplishing labour-intensive jobs and complex multi-tasking operations. Design complexities and cost considerations are critical in restricting researchers from deploying systems with more than two arms. On the other hand, while mobile manipulators equipped with numerous arms,[9] may have enhanced versatility and productivity, factors such as complexities in control, coordination, weight and collisions between arms could affect the robot's stability and lead to difficulties in operating effectively. Therefore, having four arms distributed and mounted evenly on a mobile manipulator's base strikes an optimal balance and centre of gravity.[10]

The emergence of a car-like mobile robot equipped with four arms represents a transformative step in automating industrial and construction processes. This mechanical system is designed to perform various tasks ranging from material handling to complex assembly operations while navigating dynamic and congested workspaces. Ensuring safe, efficient, and collision-free navigation in such constrained environments enhances productivity and is critical in safeguarding human workers and infrastructure. Despite the improved stability and operational effectiveness, only a few researchers have studied four-arm robotic systems due to factors such as complexity of the control algorithms and intensive computations given the intimate coupling of the double nonholonomic constraints arising from the union of an articulated robotic arm and a mobile platform.[10,11] This warrants further research to adopt this autonomous mechanical system on a large scale, particularly in exploring its contribution to performing complex tasks autonomously in labour-intensive sectors. Moreover, when it comes to speeding up construction processes or project timelines without compromising quality and work standards, a multiple-agent system of four-arm car-like mobile manipulators working simultaneously to achieve common goals offers more excellent coverage and efficiency than a single unit, as each manipulator can independently perform assigned tasks across the workspace.[11] Apart from efficient task execution, multi-agent robotic systems can quickly adapt to changing project requirements by reallocating tasks among agents,[5,11] making them suitable for large and small construction projects. Researchers have been inspired to study multi-agent systems to accomplish complex tasks and address labour shortages.[7,8,12]

Due to the complex operation of the multi-agent system in dynamic settings, the Lyapunov-based Control Scheme (LbCS), which belongs to the classical artificial potential field method, will be utilized in this research to address the motion planning and control problem. This paper addresses the crucial task of collision-free navigation for multiple four-arm car-like manipulators, aiming to enhance the capabilities of multi-agent robotic systems operating in dynamic and potentially hazardous or high risk construction sites. By introducing innovative acceleration-based motion controllers derived using LbCS for the car-like mobile robots and their revolute arms, this study provides promising solutions for autonomously addressing shortages in labour-intensive industrial and construction sectors. The main contributions of this paper are:

- *Design of a new multi-agent system of autonomous car-like vehicles comprising four robotic arms, each with two revolute links connected to an end-effector.* The combination of multiple autonomous car-like vehicles and robotic arms allows the multi-agent system to perform a wide range of construction tasks such as material handling and assembling, increasing efficiency and productivity. In comparison to the collaborative robotic systems,[8,11,12] the proposed multi-agent system can be scaled up or down according to the construction project's needs and can speed up construction processes due to the enhanced flexibility offered by each unit's four arms.
- *Design of Lyapunov-based acceleration controllers to attain collision-free navigation for a multi agent system of four-arm car-like manipulators in a dynamic environment.* Compared to robotic systems that utilize velocity-based motion controllers which may lead to erratic movement due to sudden changes in angular velocities,[6,13] the acceleration-

based controllers assure smooth trajectory and motion. The derived controllers allow for seamless coordination and collaboration among the agents and avoid obstacles, enhancing the robotic system's overall performance and productivity in executing multiple tasks.

The remainder of this paper is organized as follows: Section 2 reviews the literature relevant to the navigation of autonomous multi-agent systems. Then, Section 3 describes the methodology adopted in this paper to facilitate autonomous navigation. The system modelling and kinematic analysis of the multi-agent system are provided in Section 4. The system's work environment details are presented in Section 5, while the acceleration-based controllers are designed in Section 6. Next, Section 7 analyses the system's stability, while Section 8 provides the Convergence Analysis. Then, Section 9 presents the results of experimental validations conducted in simulated environments designed to mimic real world industrial settings. After that, Section 10 discusses the implications of the findings and explores potential applications. Finally, Section 11 concludes with a summary of the results, contributions to the field, and an outline of future research directions.

2. Literature review

Robotics researchers continuously focus on harnessing the diverse capabilities of multi-agent robotic systems to foster better performance and broader workspace coverage. Despite the computational complexities and challenges in finding precise autonomous navigation mechanisms, the research mainly focuses on deploying the multi-agents effectively for enhanced efficiency and scalability in operations. As a result, several multi-agent robotics systems have been proposed and utilized to ensure enhanced autonomy and fluent task execution in specific environments. This literature review overviews the multi-agent robotic systems used to execute specific tasks in construction settings.

The pioneer of construction robots can be traced back to its utilization in prefabricated manufacturing in the 1960s. [1] However, it was mainly limited to handheld machinery-assisted workers who could complete manual operations with limited automation and lower productivity. The recent application of robotics in construction has enabled the use of multi-agent systems to carry out complex material handling tasks that involve gathering, transportation, and assembly of materials. In 2019, Sartoretti *et al*.[12] used the actor-critic algorithm to a distributed construction problem whereby multiple TERMES robots, each equipped with a 2-link robotic arm connected to an end-effector, worked collaboratively to gather and place simple block elements to build a user-specified structure in a shared environment. A year later, Krizmancic *et al*.[5] proposed a decentralized task planning and coordination framework for a cooperative aerial-ground robotic team to automate construction tasks like locating, picking, transporting and assembling brick-like objects to build predefined structures. The Generalized Partial Global Planning method was utilized to control the motion of the system comprising unmanned aerial vehicles (UAVs) and a car-like mobile manipulator with a 2-link robotic arm. The authors successfully used the multi-agent system to automate construction tasks under different multi-criteria objectives.

According to Hartmann *et al*.,[7] construction robotics is a growing industry, and studies must be conducted on the algorithmic aspects of integrating multiple specialized robots as a heterogeneous system for automating construction tasks. Moreover, they used the logic-geometric programming framework and rapidly exploring random trees methods to solve the multi-robot motion planning problem for a heterogeneous robot team comprising an anchored robotic arm and several single-arm mobile manipulators.[7] In 2020, Wallance *et al*.[14] created a virtual teleoperation framework by integrating Genetic Algorithms and Particle Swarm Optimization with robot operating systems to control heterogeneous robots performing different construction tasks. The heterogeneous system consisted of DRC-Hubo robots for manipulating the specific construction task and Spot robots for delivering items to a waypoint. The sampling-based path planning was successfully combined with joint mode switch optimization to solve for manipulation constraints and address the task and motion planning for construction assembly tasks, including the rearrangement of objects. In contrast, Kennel-Maushart *et al*.[8] in 2023 attempted to integrate the proportional gain control method and the Reciprocal Velocity Obstacle (RVO) algorithm with a Microsoft HoloLens headset and a Samsung Galaxy Tablet using a heterogeneous system of small differential-drive robots for navigation in dynamic construction settings. The authors encountered difficulties in achieving desired trajectories and pointed out that the obstacle avoidance of RVO played a crucial role in preventing task completion. These studies depict that implementing obstacle avoidance techniques for successfully integrating multi-robotic systems in dynamic environments is indeed challenging.

To perform operations such as monitoring, surveillance, and inspection of construction sites, multi agent systems of UAVs are mainly used because they are fast, safe, and agile. In 2021, Kuru deployed a multi-robot UAV swarm system equipped with 4G and 5G technologies using agent-based dynamic route planning algorithms to complement

communication infrastructure and perform aerial surveillance operations of construction sites comprising valuable items.[4] Moreover, in 2023, Akinsemoyin *et al*.[15] used UAVs and deep learning algorithms to collect and analyze safety activity metrics for improving construction safety performance. Computer vision was used to obtain digital images of construction safety activities on active construction sites, and object detection deep-learning algorithms comprising convolutional neural networks and YOLOv3 algorithms were used for analyzing the visual imagery.

Recent advancements in AI and ML have significantly enhanced the capabilities of multi-agent robotic systems, enabling them to achieve higher levels of autonomy, adaptability and efficiency in construction settings. In 2024, Miron *et al*.[16] presented a decentralized and asymmetric multi-agent deep learning approach to enhance collaboration and collision avoidance in construction site environments. To attain collision-free navigation, trained AI agents and heuristics were evaluated and tested in environments comprising visual noise and localization errors. A similar network training approach was utilized by Li *et al*.[17] to track multiple targets in unknown environments. A multi-mode filtering target tracking method for mobile robots using deep multi-agent reinforcement learning (DMARL) was presented through a continuous learning and updating strategy. The path planning and obstacle-avoidance capabilities of heuristic algorithms were fully harnessed by Chaudhary *et al*.[18] who addressed the drawbacks of hybrid algorithms comprising ant colony optimization studied, which could only avoid static obstacles, by integrating bat optimization and LbCS. This new Bat-LbCS hybrid algorithm was effective in handling dynamic obstacles.[19]

Furthermore, integrating advanced technologies, including computer vision and sensors, has revolutionized robotic systems' collision-avoidance, mapping and collaboration capabilities. Hosmer *et al*.[20] proposed a framework for autonomous collaborative construction through modular robotic material eco-systems trained with DMARL. The authors addressed vital construction tasks by integrating cyber-physical control with visual sensory feedback and adaptive intelligence, including collaborative modular robotic assembly of reconfigurable building parts. A sensor-based obstacle-avoidance strategy was proposed recently by Kumar *et al*.,[21] who designed stabilizing acceleration controllers for an autonomous kids' personal transporter that could function as an assistive and entertainment robot. These advancements highlight the ongoing evolution of robotic systems toward greater intelligence, flexibility and operational effectiveness in complex environments.

This literature search reveals extensive research on motion planning and control algorithms of multi-agent robotic systems for construction operations has been done. Compared to the navigation techniques of multi-agent robotic systems discussed above, this paper presents a new multi-agent system of four-arm car-like mobile manipulators with acceleration-based motion controllers derived using the method of LbCS. The proposed system can speed up construction processes with increased flexibility and functionality. Thus, integrating such mobile manipulator systems in the construction sector offers enhanced operational efficiency and can revolutionize development and maintenance practices in dynamic environments.

3. An overview of LbCS

Robotic systems depend on motion control algorithms to execute movements for specific assigned tasks. One of the most effective and efficient motion control algorithms is the LbCS. This Artificial Potential Field technique has been an effective tool for nonlinear control system design and analyzing motion controllers for various robotic systems.

For navigation in a workspace, LbCS allows a robot, which is treated as a positively charged particle, to move towards its negatively charged target, aided by attractive functions. In contrast, obstacle avoidance is achieved by designing repulsive potential functions as ratios with the obstacle avoidance function in the denominator of each ratio and a positive tuning parameter in the numerator. The underlying principle in the controller design process relies on the mathematical interpretation that if a robotic system's total energy dissipates, then the system's states will ultimately reach an equilibrium point of zero energy.

This research uses LbCS to derive a Lyapunov function and extract the acceleration-based motion controllers to guide the multi-agent system of mobile manipulators to their targets while avoiding obstacles and collisions. A general framework for the Lyapunov-based motion controllers of the multi-agent system utilized in this research and an overview of the control process are shown in Fig. 1.

Fig. 2 illustrates a 3-dimensional visualization and contour plot of the Lyapunov function for autonomous navigation. A robot initially positioned at (8,8), navigates to a target at (130,130) while successfully avoiding three obstacles which are located at (50,100), (80,60) and (90,110).

4. System description and kinematic modeling

The multi-agent system consists of $k \in N$ car-like mobile platforms whereby $i \in \{1,2,3,\ldots,k\}$, and each is equipped with four robotic arms comprising revolute joints attached to

an end-effector. The cartesian coordinates of the i^{th} four-arm car-like robot of the system are denoted as $\kappa_i = (x_{ci}(t), y_{ci}(t))$. The mobile base of each robot is rectangular-shaped, resembling a car-like vehicular frame of axle length L and width W, with an orientation angle of $\phi_{ci}(t)$ taken from the z_1 axis. Two robotic arms are mounted on the ends of the front axle, while the other two are mounted on the ends of the rear axle. Each arm has two links with the 2^{nd} links connected to an end-effector, which interacts with the 2D environment to carry out designated tasks. The joints of all the robotic arms are revolute, implying excellent manoeuvrability due to the rotary joints. Taking $n \in \{1, 2, 3, 4\}$ for each of the four arms, all the 1^{st} links are denoted as r_{in1} and the 2^{nd} links are denoted as r_{in2}.

Moreover, all the 1^{st} and 2^{nd} revolute link angles of each vehicle are measured anticlockwise from its longitudinal axis and are labelled as $\phi_{in1}(t)$ and $\phi_{in2}(t)$, respectively. The system model of the i^{th} agent is shown in Fig. 3, where the four arms of the system are labelled as Arm $i1$, Arm $i2$, Arm $i3$, and Arm $i4$. For the i^{th} agent, its nonholonomic mobile platform and the 2-link nonholonomic arms are considered as one complete robot unit. To ensure a safe distance between the arms and avoid inter-arm collisions, the following assumptions are made with respect to Fig. 3:

Assumptions:

1. $r_{i12} + r_{i41} < L - 2\epsilon_1$
2. $r_{i21} + r_{i31} < L - 2\epsilon_1$
3. $r_{in2} \leq \sqrt{\left(\frac{L}{2} + \epsilon_1\right)^2 + (\epsilon_2)^2}$

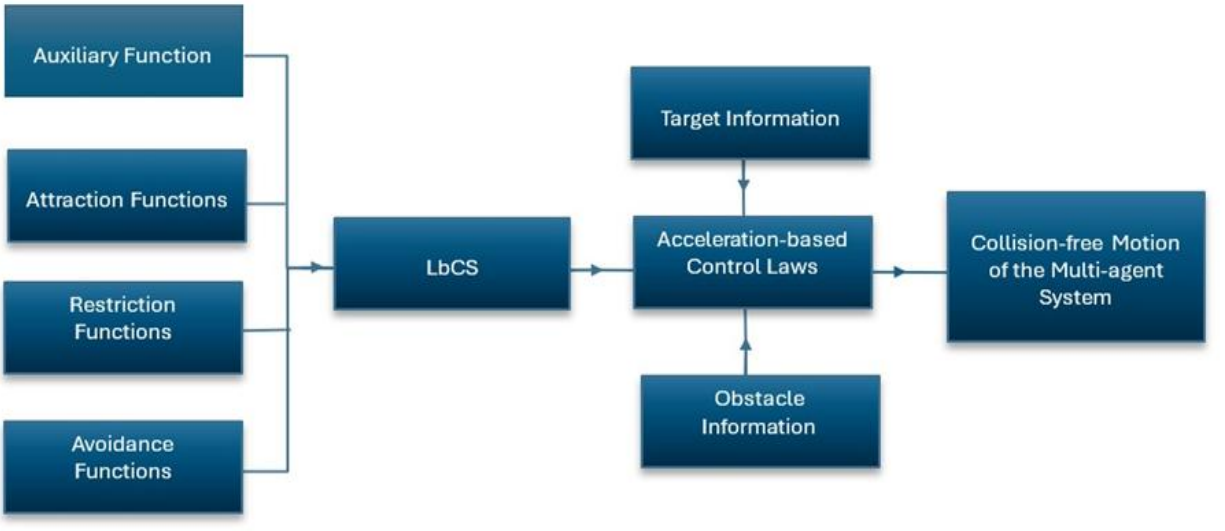

Fig. 1: Block diagram illustrating the control inputs and the control process.

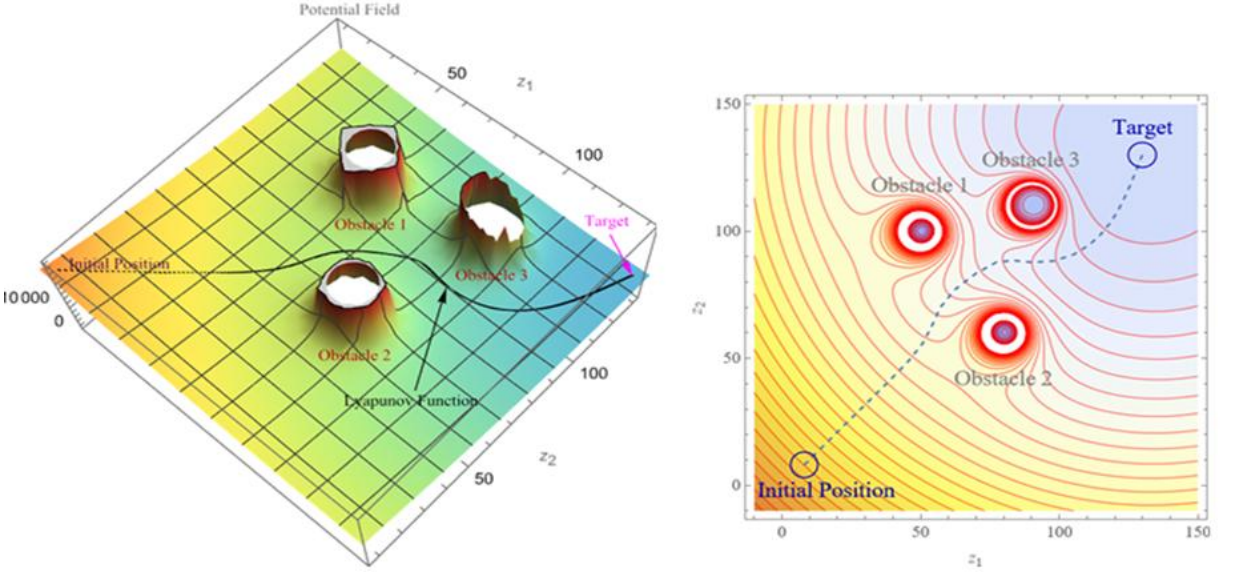

Fig. 2: A demonstration of LbCS in a workspace with three obstacles.

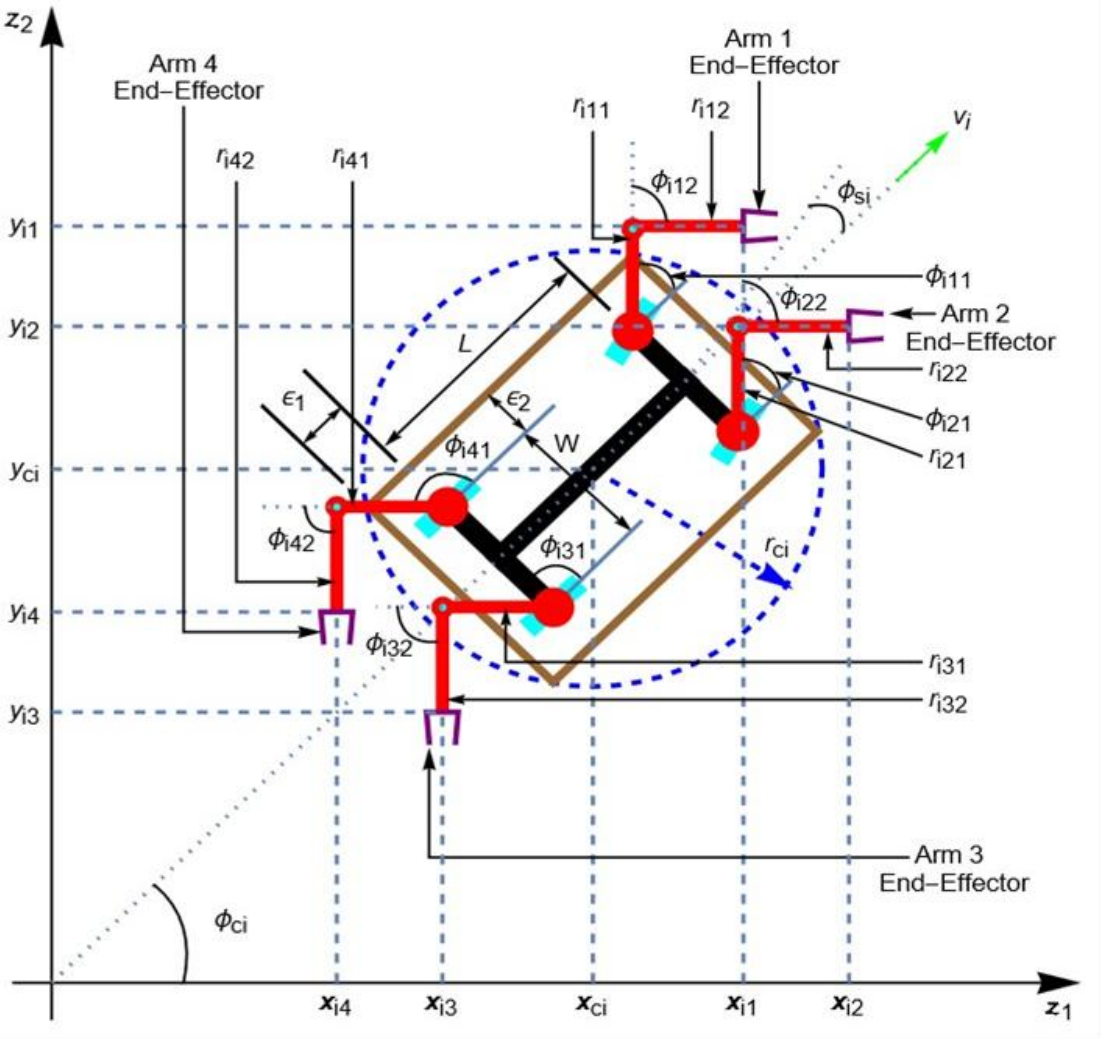

Fig. 3: Schematic representation of the i^{th} mobile manipulator in the z_1z_2 plane.

The coordinates of each robotic arm end-effector of the i^{th} agent for $n \in \{1,2,3,4\}$ are (x_{in}, y_{in}), and can be collectively described as a set of equations given in Eqs. (1) and (2) below:

$$x_{in} = x_{ci} + A\frac{L}{2}\cos\phi_{ci} - B\frac{W}{2}\sin\phi_{ci} + \sum_{n=1}^{4}\sum_{m=1}^{2} r_{inm}\cos\vartheta \quad (1)$$

$$y_{in} = y_{ci} + A\frac{L}{2}\sin\phi_{ci} + B\frac{W}{2}\cos\phi_{ci} + \sum_{n=1}^{4}\sum_{m=1}^{2} r_{inm}\sin\vartheta \quad (2)$$

where $A = (-1)^{\left\lceil\frac{n}{2}\right\rceil-\left\lceil\frac{n}{4}\right\rceil}$, $B = (-1)^{\left\lfloor\frac{n}{2}\right\rfloor}$, and $\vartheta = \phi_{ci} + \sum_{l=1}^{m}(\phi_{inl})$.

The coordinate (x_{in}, y_{in}), where $i \in \{1,2,3,\ldots,k\}$ and $n \in \{1,2,3,4\}$, describes how the coordinates of each end-effector are influenced by the position and orientation of each robot's chassis, the lengths of revolute links, and the joint angles. They allow for the calculation of the end-effector positions based on these parameters as follows:

- The coefficient $(-1)^{\left\lceil\frac{n}{2}\right\rceil-\left\lceil\frac{n}{4}\right\rceil}$ alternates between 1 and -1 based on the value of $\left\lceil\frac{n}{2}\right\rceil - \left\lceil\frac{n}{4}\right\rceil$. This term contributes to the x-coordinate based on the length L and the orientation of the end-effector.
- The coefficient $(-1)^{\left\lfloor\frac{n}{2}\right\rfloor}$ alternates between 1 and -1 based on the value of $\left\lfloor\frac{n}{2}\right\rfloor$. This term contributes to the x-coordinate based on the width W and the orientation of the end-effector.
- The y_{in} coordinate follows a similar pattern as above, with corresponding terms involving the y-coordinate y_{ci}.

Each agent in the multi-agent system is enclosed in a circular protective region centred at $(x_{ci}(t), y_{ci}(t))$ with radius $r_{ci} = \sqrt{\left(\frac{L}{2}+\epsilon_1\right)^2 + \left(\frac{W}{2}+\epsilon_2\right)^2}$ as shown in Fig. 3. This approach of enclosing a robot in a protective region has been

adopted from Vanualailai *et al.*[13] and is implemented in this research as this procedure provides the individual agents with maximized free space to operate in dynamic environments. The constants ϵ_1 and ϵ_2 are the clearance parameters for the i^{th} vehicle. They are added to the dimensions L and W to ensure that there is always a safe distance as the multiple agents safely steer past each other and the obstacles.

The dimensions and maximum steering angle $\phi_{si_{max}}$ of each agent in the multi-agent system are kept the same. To control the system's motion in a dynamic environment, it is essential to consider the kinematics in the design of the control algorithm. For simplicity, we assume that the two wheels on each axis (front and rear) collapse into a single wheel located at the midpoint of the axis. This implies that the nonholonomic constraints of all four wheels of the i^{th} mobile manipulator are subject to two nonholonomic constraints, one for the two front wheels and one for the two rear wheels. The front wheel can be steered while the rear wheel orientation is fixed. The nonholonomic constraints have been inherently reflected in the ordinary differential equations. For each mobile manipulator, it is assumed that $\phi_{si}(t) = \phi_{ci}(t)$ and there is no slippage and pure rolling because the velocities perpendicular to the wheels are zero, as expressed by the set of equations in Eqs. (3) and (4) below: [6,13]

$$\dot{x}_{wi_R} \sin\phi_{ci} - \dot{y}_{wi_R} \cos\phi_{ci} = 0 \tag{3}$$

$$\dot{x}_{wi_F} \sin(\phi_{ci} + \phi_{si}) - \dot{y}_{wi_F} \cos(\phi_{ci} + \phi_{si}) = 0 \tag{4}$$

where $(\dot{x}_{wi_R}, \dot{y}_{wi_R})$ and $(\dot{x}_{wi_F}, \dot{y}_{wi_F})$ are the rear and front wheel velocities of the i^{th} car-like vehicle, respectively. Therefore, the configuration vector for the i^{th} unit of the multi-agent system is given as $x_{ci}(t), y_{ci}(t), \phi_{ci}(t), \phi_{in1}(t), \phi_{in2}(t) \in R^3$.

The kinematic model of the i^{th} car-like platform, for $n \in \{1,2,3,4\}$, on suppressing t, which is described collectively as a set of equations in Eqs. (5)-(8) given as:

$$\dot{x}_{ci} = v_i \cos\phi_{ci} - \frac{L}{2} w_i \sin\phi_{ci} \tag{5}$$

$$\dot{y}_{ci} = v_i \sin\phi_{ci} + \frac{L}{2} w_i \cos\phi_{ci} \tag{6}$$

$$\dot{\phi}_{ci} = w_i := \frac{v_i}{L} \tan\phi_{si} \tag{7}$$

$$\dot{v}_i = \mu_i, \dot{w}_i = \varpi_i \tag{8}$$

while those of each robotic arm are given in Eqs. (9)-(12) as:

$$\dot{x}_{in} = v_i \cos\phi_{ci} - \left[(-1)^{\left\lceil \frac{n}{2} \right\rceil - \left\lceil \frac{n}{4} \right\rceil}\right] L w_i - \left[(-1)^{\left\lceil \frac{n}{2} \right\rceil}\right] \frac{W}{2} w_i \cos\phi_{ci} - (w_{ci} + \sum_{n=1}^{4}\sum_{l=1}^{m} w_{inl}) \sum_{u=1}^{l-1} r_{inu} sin(\phi_{ci} + \sum_{m=1}^{u} \phi_{inm}) \tag{9}$$

$$\dot{y}_{in} = v_i \sin\phi_{ci} + \left[(-1)^{\left\lceil \frac{n}{2} \right\rceil - \left\lceil \frac{n}{4} \right\rceil}\right] L w_i - \left[(-1)^{\left\lceil \frac{n}{2} \right\rceil}\right] \frac{W}{2} w_i \sin\phi_{ci} + (w_{ci} + \sum_{n=1}^{4}\sum_{l=1}^{2} w_{inl}) \sum_{u=1}^{l-1} r_{inu} \cos(\phi_{ci} + \sum_{m=1}^{u} \phi_{inm}) \tag{10}$$

$$\dot{\phi}_{\text{in}1} = w_{in1}, \dot{\phi}_{in2} = w_{in2} \tag{11}$$

$$\dot{w}_{in1} = \sigma_{in1}, \dot{w}_{in2} = \sigma_{in2} \tag{12}$$

The angular and translational velocities are $w_i(t)$ and $v_i(t)$, while the angular and translational accelerations are $\varpi_i(t)$ and $\mu_i(t)$, which also are the acceleration-based controllers of each car-like mobile base of the system. The end-effector coordinates of the k^{th} robotic arm for $k \in \{1,2,3,4\}$ is given in Eq. (13) as

$$\boldsymbol{x}_{ik} = \begin{bmatrix} x_{ik}(t) \\ y_{ik}(t) \end{bmatrix} \tag{13}$$

Subsequently, with respect to the i^{th} individual agent shown in Fig. 3, the end-effector positions of all the robotic arms of the multi-agent system can be represented in matrix form as given in Eq. (14) as follows:

$$\boldsymbol{x}_{ik} = \begin{bmatrix} \boldsymbol{x}_{i1}(t) \\ \boldsymbol{x}_{i2}(t) \\ \boldsymbol{x}_{i3}(t) \\ \boldsymbol{x}_{i4}(t) \end{bmatrix} \tag{14}$$

For $i \in \{1,2,3,\dots,k\}$ and $n \in \{1,2,3,4\}$, the angular velocities of the robotic arms of the i^{th} agent are denoted as w_{in1} and w_{in2}, while the angular accelerations are given by σ_{in1} and σ_{in2}, which also are the acceleration-based controllers of the 2-link robotic arms of each manipulator.

The initial condition of the proposed multi-agent system where $n \in \{1,2,3,4\}$, upon suppressing t, is given below in Eq. (15) as:

$$\mathbf{x}_0 := x(t_0) := (x_{ci_0}, y_{ci_0}, x_{in_0}, y_{in_0}, \phi_{ci_0}, \phi_{in1_0}, \phi_{in2_0},) \in R^{n+7} \tag{15}$$

Subsequently, the state vector of the system is given in Eq. (16) as:

$$\mathbf{x} := (x_{ci}, y_{ci}, x_{in}, y_{in}, \phi_{ci}, \phi_{in1}, \phi_{in2}) \in R^{n+7} \tag{16}$$

5. Navigating in the dynamic workspace

The planar workspace is a fixed, closed, and bounded

rectangular region in the z_1z_2 plane cluttered with obstacles of various sizes. Based on the work requirements and target locations, $k \in N$ car-like mobile manipulators can be utilized as a multi-agent system to perform designated tasks. Each mobile manipulator must navigate to its target in the dynamic workspace while avoiding each other and the obstacles in a dual-step motion as described in Algorithm 1. Four assigned tasks can be performed at the end-effector targets by each manipulator; however, the car-like vehicle must park at a specific location close to these targets so that the robotic arms can easily access them for task execution. In this research, the precise location of this parking spot is known as the pseudo-target. Thus, each agent of the multi-agent system can be tagged with four end-effector targets and a pseudo-target.

Definition 5.1 The pseudo-target for the i^{th} car-like vehicle is a disk-shaped region centred at $x_{T_{ci}} = (a_{ci}, b_{ci})$ with radius $\zeta_{T_{ci}}$, and described below in Eq. (17) as:

$$T_{ci} = \{(z_1, z_2) \in R^2 : (z_1 - a_{ci})^2 + (z_2 - b_{ci})^2 \leq \zeta_{T_{ci}}^2\} \quad (17)$$

Definition 5.2 The end-effector targets for the n^{th} robotic arm of the i^{th} car-like mobile manipulator are disk-shaped with center $x_{T_{in}} = (a_{in}, b_{in})$ and radius $\varsigma_{T_{in}}$ where $n \in \{1,2,3,4\}$, and are given below in Eq. (18) as:

$$T_{in} = \{(z_1, z_2) \in R^2 : (z_1 - a_{in})^2 + (z_2 - b_{in})^2 \leq \varsigma_{T_{in}}^2\} \quad (18)$$

For efficient navigation in dynamic construction environments, the agents in the multi-agent system may encounter several fixed obstructions, such as structural elements, debris and items lying around construction sites and factories, that can obstruct the agents' paths and challenge their operation. In this paper, these obstacles are treated as disks.

Definition 5.3 The $h \in N$ obstacles in this research are generally represented as disks, centred at $x_{O_q} = (o_{q1}, o_{q2})$ with radius $r_{O_q} > 0$ where $q \in \{1,2,3,...,h\}$, and described as Eq. (19):

$$O_q = \{(z_1, z_2) \in R^2 : (z_1 - o_{q1})^2 + (z_2 - o_{q2})^2 \leq r_{O_q}^2\} \quad (19)$$

Definition 5.4 The multi-agent system's equilibrium state is in Eq. (20):

$$\mathbf{x}_E^* := (a_{in}, b_{in}, \phi_{ci}^*, \phi_{in1}^*, \phi_{in2}^*) \in R^{n+7} \quad (20)$$

The multi-agent system's navigation from the initial positions to assigned targets is described in Algorithm 1. In steps 1 and 2, the end-effector target and pseudo-target information are set to the system. The obstacle information is included in Step 3. Then, the system's motion is initialized in Step 4 as the car-like platforms manoeuvre to the respective pseudo-targets, after which the end-effectors reach their targets to carry out designated tasks in Step 5. The function Ψ_i, given in Eq. (23), is utilized to ensure that the end-effectors are not attracted to their targets, (a_{in}, b_{in}), until the centre of the mobile bases have safely entered inside a region within a user-defined distance of $r_i > 0$ from the pseudo-targets.

Algorithm 1: Dual-step motion of the multi-agent system.

Step 1 Assign end-effector targets (a_{in}, b_{in})

Step 2 Define (a_{ci}, b_{ci}) as pseudo-targets for each car-like vehicle

Step 3 Activate obstacle avoidance scheme for the system

Step 4 Initialize movement of the car-like vehicles from their original positions to (a_{ci}, b_{ci})

```
while r_i > 0 do
    if ψ_i = 0 then
       Only the car-like vehicles move - the arms are not attracted to their targets;
    else
       nothing
       Step 5  Initialize movement of the end-effectors to perform assigned tasks
            if ψ_i ≤ r_i^2 − ‖κ_i − x_{T_ci}‖^2 then
               End-effectors navigate to (a_in, b_in) ;
            else
               nothing
            end if
    end if
end while
```

6. Design of the Lyapunov-based acceleration controllers

6.1 Lyapunov function components

Definition 6.1 The potential function for attraction of the i^{th} car-like vehicle to its pseudo-target is described in Eq. (21) as:

$$A_i(\boldsymbol{x_i}) = \frac{1}{2}\left(\left\|\boldsymbol{\kappa}_i - \boldsymbol{x}_{T_{ci}}\right\|^2 + v_i^2 + w_i^2\right) \quad (21)$$

Definition 6.2 The attraction function that facilitates the convergence of the system's articulated arm end-effectors to their assigned targets is given in Eq. (22) as:

$$B_i(\boldsymbol{x}_i) = \frac{\Psi_i}{2}\left(\sum_{n=1}^{4}\left\|\boldsymbol{x}_{in} - \boldsymbol{x}_{T_{in}}\right\|^2 + \sum_{n=1}^{4}\sum_{m=1}^{2} w_{inm}^2\right) \quad (22)$$

where

$$\Psi_i = \begin{cases} 0, & \left\|\boldsymbol{\kappa}_i - \boldsymbol{x}_{T_{ci}}\right\|^2 > r_i^2 \\ r_i^2 - \left\|\boldsymbol{\kappa}_i - \boldsymbol{x}_{T_{ci}}\right\|^2, & otherwise \end{cases} \quad (23)$$

Definition 6.3 The obstacle avoidance function that ensures that the i^{th} mobile manipulator avoids collisions with the q^{th} fixed obstacle where $q \in \{1, 2, 3, \dots, h\}$ is described in Eq. (24) as:

$$H_{iq}(\boldsymbol{x}) = \frac{1}{2}\left(\left\|\boldsymbol{\kappa}_i - \boldsymbol{x}_{O_q}\right\|^2 - \left(r_{ci} + r_{O_q}\right)^2\right) \quad (24)$$

Each agent of the multi-agent system must avoid all the other agents in the dynamic workspace, implying that a moving car-like vehicle becomes a dynamic obstacle to all the other car-like vehicles in the workspace and has to be treated as a moving obstacle for all the other agents. Thus, the j^{th} mobile manipulator becomes a moving obstacle for the i^{th} mobile manipulator.

Definition 6.4 The repulsive potential field function for the inter-robot avoidance within the multi-agent system for $j \neq i$ is described in Eq. (25) as:

$$C_{ij}(\boldsymbol{x}) = \frac{1}{2}\left(\left\|\boldsymbol{\kappa}_i - \boldsymbol{\kappa}_j\right\|^2 - (2r_{ci})^2\right) \quad (25)$$

6.2 Restrictions and limitations

All the car-like vehicles in the multi-agent system are driven by their rear wheels and steered using their front wheels. Every car-like system must comply with the vehicle's velocity and steering angle limitations. The construction of the artificial obstacles for each singularity and restriction as a prerequisite to use LbCS is adopted from.[6]

Definition 6.5 The restriction on the steering angle for each mobile manipulator is given as $\phi_{si}(t) \leq \phi_{si_{max}} < \frac{\pi}{2}$ where $\phi_{si_{max}}$ is the maximum steering angle, and is facilitated by Eq. (26):

$$|si| < \frac{v_{i_{max}}|\tan\phi_{si_{max}}|}{L} := si_{max} \quad (26)$$

Definition 6.6 The function P_{vi}, which guarantees that the i^{th} car-like mobile base adheres to the linear velocity restrictions is given as Eq. (27):

$$P_{vi} = \frac{1}{2}\left(v_{i_{max}}^2 - v_i^2\right) \quad (27)$$

Definition 6.7 The function that controls the angular velocity of the i^{th} car-like mobile base is in Eq. (28):

$$P_{wi} = \frac{1}{2}\left(\left(\frac{v_{i_{max}}}{L}\tan\phi_{w_{i_{max}}}\right)^2 - w_i^2\right) \quad (28)$$

Given $v_{i_{max}}$ and $w_{i_{max}}$ are the maximum linear and angular velocities of the i^{th} car-like platform, the linear and angular velocities are restricted as $v(t) \leq v_{max}$ and $w(t) \leq w_{max}$.

Definition 6.8 The function that controls the angular velocities of the 1^{st} and 2^{nd} revolute links of each robotic arm of the i^{th} car-like mobile base, where $w_{in1}(t) \leq w_{in1_{max}}$ and $w_{in2}(t) \leq w_{in2_{max}}$ for $n \in \{1,2,3,4\}$, *is* given as Eq. (29):

$$Q_{in} = \frac{1}{2}\left(\sum_{n=1}^{4}\left(w_{in1_{max}}^2 - w_{in1}^2\right) + \sum_{n=1}^{4}\left(w_{in2_{max}}^2 - w_{in2}^2\right)\right) \quad (29)$$

The 2^{nd} links of all articulated arms cannot fully fold onto their corresponding 1^{st} links while performing either clockwise or counterclockwise rotation. The singularities of the 2^{nd} links of all the arms arise when $\phi_{in2} = |\phi_{in2_{max}}|$, and the function given below is utilised to account for these singularities in Eq. (30):

$$S_{in} = \phi_{in2_{max}} - |\phi_{in2}| \quad (30)$$

where $n \in \{1,2,3,4\}$.

6.3 Lyapunov function

In accordance with LbCS, a Lyapunov function that is suitable for Eqs. (5)-(12) can be constructed by combining all the attractive and repulsive potential functions. Introducing the positive real numbers ρ_{in}, ϱ_i, λ_i, γ_{iq}, ξ_{ij} and β_{in} as the control parameters, a Lyapunov function, for $i \in \{1,2,3,\dots,k\}$, $j \in \{1,2,3,\dots,k\}$, $n \in \{1,2,3,4\}$ and $q \in \{1,2,3,\dots,h\}$, can be defined as:

$$\pounds(\boldsymbol{x}) = \sum_{i=1}^{k}\left(A_i(\boldsymbol{x}_i) + B_i(\boldsymbol{x}_i) + D_i(\boldsymbol{x}_i)\left(\frac{\varrho_i}{P_{vi}} + \frac{\lambda_i}{P_{wi}} + \sum_{q=1}^{h}\frac{\gamma_{iq}}{H_{iq}} + \sum_{n=1}^{4}\frac{\rho_{in}}{Q_{in}} + \sum_{n=1}^{4}\frac{\beta_{in}}{S_{in}} + \sum_{\substack{j=1 \\ i\neq j}}^{k}\frac{\xi_{ij}}{C_{ij}}\right)\right) \quad (31)$$

To guarantee the nonlinear controllers vanish at the targets, an auxiliary function is utilized in Eq. (31) and is described as:

$$D_i(\boldsymbol{x_i}) = \frac{1}{2}\left(\left\|\boldsymbol{\kappa}_i - \boldsymbol{x}_{T_{ci}}\right\|^2\right) + \frac{\Psi_i}{2}\left(\sum_{n=1}^{4}\left\|\boldsymbol{x}_{in} - \boldsymbol{x}_{T_{in}}\right\|^2\right) \quad (32)$$

The term $\left\|\boldsymbol{\kappa}_i - \boldsymbol{x}_{T_{ci}}\right\|^2$ in Eq. (32) assures that the platforms of the mobile manipulators converge to their targets which will ensure that at some point in time, $\left\|\boldsymbol{\kappa}_i - \boldsymbol{x}_{T_{ci}}\right\|^2 \leq r_i^2$. This will ensure that the end-effectors of the manipulators' arms will reach their assigned targets and, therefore, will address the goal non-reachable with obstacles nearby (GNRON) problem.

6.4 Design of the controllers

The various components of $\pounds(\boldsymbol{x})$, for $i \in \{1,2,3,\ldots,k\}$, are differentiated separately with respect to t to extract the nonlinear controllers for Eqs. (5)-(12) to obtain Eq. (33):

$$\dot{\pounds}(\boldsymbol{x}) = \sum_{i=1}^{k}\Bigg(\dot{A}_i(\boldsymbol{x}_i) + \dot{B}_i(\boldsymbol{x}_i) + \dot{D}_i(\boldsymbol{x}_i)\left(\frac{\varrho_i}{P_{vi}} + \frac{\lambda_i}{P_{wi}} + \sum_{q=1}^{h}\frac{\gamma_{iq}}{H_{iq}} + \sum_{n=1}^{4}\frac{\rho_{in}}{Q_{in}} + \sum_{n=1}^{4}\frac{\beta_{in}}{S_{in}} + \sum_{\substack{j=1\\ i\neq j}}^{k}\frac{\xi_{ij}}{C_{ij}}\right)\Bigg) -$$

$$\sum_{i=1}^{k}\Bigg(D_i(\boldsymbol{x}_i)\left(\frac{\varrho_i \dot{P_{vi}}}{P_{vi}^2} + \frac{\lambda_i \dot{P_{wi}}}{P_{wi}^2} + \sum_{q=1}^{h}\frac{\gamma_{iq}\dot{H_{iq}}}{H_{iq}^2} + \sum_{n=1}^{4}\frac{\rho_{in}\dot{Q_{in}}}{Q_{in}^2} + \sum_{n=1}^{4}\frac{\beta_{in}\dot{S_{in}}}{S_{in}^2} + \sum_{\substack{j=1\\ i\neq j}}^{k}\frac{\xi_{ij}\dot{C_{ij}}}{C_{ij}^2}\right)\Bigg) \quad (33)$$

which, after collecting terms comprising v_i, w_i, and w_{inl}, is rearranged as Eq. (34):

$$\dot{\pounds}(\boldsymbol{x}) = \sum_{i=1}^{k}(\mathrm{F}_1 v_i + \mathrm{F}_2 w_i + \sum_{n=1}^{4}\sum_{l=1}^{2}\mathrm{F}_{inl} w_{inl})) \quad (34)$$

where the functions $\mathrm{F}_1, \mathrm{F}_2$, and F_{inl} for $i \in \{1,2,3,\ldots,k\}$, $n \in \{1,2,3,4\}$ and $l \in \{1,2\}$, upon suppressing $\mathbf{x}_i$, are in Eqs. (35)-(37):

$$\mathrm{F}_1 = \frac{\partial \pounds}{\partial x_{ci}}\cos\phi_{ci} + \frac{\partial \pounds}{\partial y_{ci}}\sin\phi_{ci} + \frac{\varrho_i D_i}{P_{vi}{}^2}\mu_i + \mu_i \quad (35)$$

$$\mathrm{F}_2 = \frac{\partial \pounds}{\partial y_{ci}}\frac{L}{2}\cos\phi_{ci} - \frac{\partial \pounds}{\partial x_{ci}}\frac{L}{2}\sin\phi_{ci} + \frac{\partial \pounds}{\partial \phi_{ci}} + \frac{\lambda_i D_i}{P_{wi}{}^2}\varpi_i + \varpi_i \quad (36)$$

$$\mathrm{F}_{inl} = \frac{\partial \pounds}{\partial \phi_{inl}} + \frac{\rho_{in} D_i}{Q_{in}{}^2}\sigma_{inl} + \sigma_{inl} \quad (37)$$

6.5 Control laws

The acceleration-based motion controllers for the i^{th} four-arm car-like mobile manipulator are μ_i, ϖ_i and σ_{inl}. The angular acceleration controller of each 2-link robotic arm of the entire multi-agent system is σ_{inl}, while the linear and angular acceleration controllers of each car-like vehicle are μ_i and ϖ_i, respectively. Introducing $\eta_{i_1} >, \eta_{i_2} > 0$ and $\eta_{i_{n+2}} > 0$, as the convergence parameters, these controllers are defined as Eqs. (38)-(40):

$$\mu_i = -\frac{P_{vi}^2}{P_{vi}^2 + \varrho_i D_i}\left(\cos\phi_{ci}\frac{\partial \pounds}{\partial x_{ci}} + \sin\phi_{ci}\frac{\partial \pounds}{\partial y_{ci}} + \eta_{i_1} v_i\right) \quad (38)$$

$$\varpi_i = \frac{P_{wi}^2}{P_{wi}^2 + \lambda_i D_i}\left(\frac{L}{2}\sin\phi_{ci}\frac{\partial \pounds}{\partial x_{ci}} - \frac{L}{2}\cos\phi_{ci}\frac{\partial \pounds}{\partial y_{ci}} - \frac{\partial \pounds}{\partial \phi_{ci}} - \eta_{i_2} w_i\right) \quad (39)$$

$$\sigma_{inl} = -\frac{1}{1 + \sum_{n=1}^{4}\frac{\rho_{in} D_i}{Q_{in}^2}}\left(\sum_{n=1}^{4}\sum_{l=1}^{2}\frac{\partial \pounds}{\partial \phi_{inl}} + \sum_{n=1}^{4}\sum_{l=1}^{2}\eta_{i_{n+2}} w_{inl}\right) \quad (40)$$

7. Stability analysis of the system

With respect to Eqs. (5)-(12), we get Eq. (41):

$$\dot{\pounds}(x) = -\sum_{i=1}^{k}\left(\left(\eta_{i_1} v_i^2 + \eta_{i_2} w_i^2 + \sum_{n=1}^{4}\sum_{l=1}^{2}\eta_{i_{n+2}} w_{inl}^2\right)\right) \leq 0, \forall\, x \in D\left(\pounds(x)\right) \quad (41)$$

where D is the domain on which $\pounds(x) \geq 0$, $\pounds(x)$ is a Lyapunov function on $D\left(\pounds(x)\right)$ that guarantees the stability of the proposed multi-agent system. The stability analysis is appropriately summarized in Theorem (7.1) below:

Theorem 7.1 The equilibrium point $\mathbf{x}_E^*$, as given in Eq. (20), is a stable point given the acceleration-based controllers of the multi-agent system are defined as in Eqs. (38)-(40). It is clear that $\pounds(x)$ is a continuous function, $\dot{\pounds}(x) \leq 0$, $\pounds(\mathbf{x}_E^*) = 0$ and $\dot{\pounds}(\mathbf{x}_E^*) = 0$. This implies that $\mathbf{x}_E^*$ is a stable equilibrium point of the proposed multi-agent system.

8. Convergence analysis of the system

The convergence criterion of LaSalle's invariance principle will be utilized in this section to demonstrate a theoretical exposition of the convergence of the Lyapunov-based controllers obtained in Eqs. (38)-(40). For the proposed multi-agent system, LaSalle's principle provides a framework to establish convergence to proper invariant sets or reach a steady state for the i^{th} mobile manipulator along its trajectory.

Definition 8.1 A set $D\left(\pounds(x)\right)$ is called an invariant set of Eqs. (5)-(12) if any solution $\mathbf{x}_i(t)$ which starts from a point in $D\left(\pounds(\mathbf{x})\right)$ at some time t_a also remains in $D\left(\pounds(\mathbf{x})\right)$ at all times:[22]

$$x_i(t_a) \in D\left(\pounds(\mathbf{x})\right) \Rightarrow x_i(t) \in D\left(\pounds(x)\right), \forall\, t \in R$$

This implies that the set of all equilibrium points is an invariant set. Moreover, the domain of attraction of an equilibrium point is also an invariant set. According to LaSalle,[23] bounded solutions converge to the largest invariant subset of the set where the derivative of the Lyapunov function is zero. In this research, LaSalle's invariance principle is utilized to prove that the individual solutions of the multi-agent system approach the desired final configuration in space or remain near the equilibrium state when time goes to infinity, as defined below:

Definition 8.2 Let ε and T be positive real numbers and $\mathbf{x}_i(t)$ be a function of time. Let $\mathbf{x}_E^*$ be the set of all points $p \in D\big(\pounds(\mathbf{x})\big)$ such that $\dot{\pounds}(p) = 0$.[23] Then, $\mathbf{x}_i(t)$ approaches a set $\mathbf{x}_E^*$ as t approaches infinity, denoted by $\mathbf{x}_i(t) \to x_E^*$ as $t \to \infty$, if $\forall \varepsilon > 0, \exists\, T > 0, \forall\, t > T, \exists\, p \in \boldsymbol{x}_E^*, \| x_i(t) - p \| < \varepsilon$.

As appropriately stated in Theorem (7.1) and illustrated in Fig. 4(c), $\pounds(\mathbf{x})$ gradually vanishes as Eq. (42):

$$\lim_{t \to +\infty} \pounds(x) = 0 \tag{42}$$

which is the lower bound of $\pounds(\mathbf{x})$.

Theorem 8.3 Suppose there is a scalar function $\pounds(\mathbf{x})$ defined as in Eq. (31) which has continuous first order partial derivatives in $D\big(\pounds(\mathbf{x})\big)$ and is such that $\dot{\pounds}(p) \le 0$ in $D\big(\pounds(\mathbf{x})\big)$. Let $\mathbf{x}_E^*$ be the set of points $p \in D\big(\pounds(\mathbf{x})\big)$ such that $\dot{\pounds}(p) = 0$. Let $N \in D\big(\pounds(\mathbf{x})\big)$ and $\mathbf{x}_E^*$ be the largest invariant set in N. Then, $\exists$ a solution $\mathbf{x}_i$ starting in $D\big(\pounds(\mathbf{x})\big)$ such that $\mathbf{x}_i(t) \to \mathbf{x}_E^*$ as $t \to \infty$.

Proof: Let $\mathbf{x}_i(t)$ be a function of time. By continuity of Eq. (31), the function $\pounds\big(\boldsymbol{x}(t)\big)$ is bounded. Since $\dot{\pounds}(\mathbf{x}) \le 0, \forall\, \mathbf{x}_i \in D\big(\pounds(\mathbf{x})\big)$, the function $\pounds\big(\mathbf{x}(t)\big)$ is non-increasing. As a result, the limit of $\pounds\big(\mathbf{x}(t)\big)$ must exist and is finite, and is denoted as $\daleth$ using Eq. (43):

$$\lim_{t \to \infty} \pounds\big(\mathbf{x}(t)\big) = \daleth \tag{43}$$

Let an arbitrary point be $z \in \mathbf{x}_E^*$ in the ω-limit set $\mathbf{x}_E^* \subseteq N$, which is a set of points that $\pounds(z)$ approaches as time approaches infinity. Thus, by the definition of ω-limit sets, there is a sequence k_t in R such that $x_i(k_t) \to z, t \to \infty$. By the continuity of $\pounds\big(\mathbf{x}(t)\big)$, it follows that in Eq. (44):

$$\pounds(z) = \lim_{t \to \infty} \pounds\big(x(k_t)\big) = \lim_{t \to \infty} \pounds\big(x(t)\big) = \daleth \tag{44}$$

This implies that for all z in the ω-limit set $\mathbf{x}_E^*$, the function $\pounds(\mathbf{x}(t))$ has the same value in Eq. (45):

$$\pounds\big(\mathbf{x}(t)\big) = \daleth, \forall z \in \mathbf{x}_E^* \tag{45}$$

By the invariance of $\mathbf{x}_E^*$, if $z \in x_E^*$, then $x_i(t) \in x_E^*\ \forall\, t \in R$, which implies that $\pounds\big(x(t)\big) = \daleth\ \forall\, t \in R$, that is, a constant function of time, t, and must have a derivative of zero, as shown in Theorem (7.1). Hence, $\mathbf{x}_E^*$ is an invariant set, and $\mathbf{x}_i(t)$ converges to $\mathbf{x}_E^*$ as $t \to \infty$.

According to Theorem (7.1), x_E^* is stable and all individual solutions of Eqs. (38)-(40) for the multi-agent system converge to their final configurations x_E^*, where $\pounds(x_E^*) \equiv 0$, given $x_E^* \in D\big(\pounds(\mathbf{x})\big)$, as $\dot{\pounds}(\mathbf{x})$ is negative definite. While Theorem (7.1) establishes that the equilibrium point x_E^* of Eqs. (5)-(12) is stable where $\pounds(x_E^*) \equiv 0$. Theorem (8.3) sharpens this result by establishing the convergence of the bounded solutions of Eqs. (5)-(12) to the invariant set x_E^*, which is a subset of N.

9. Results and simulations

This section demonstrates the multi-agent system's capability in executing assigned tasks in constrained environments and verifies the stability results obtained from Eq. (31). The effectiveness of the proposed controllers was numerically verified using the Runge-Kutta Method, while the Wolfram Mathematica 11.2 software was used to carry out a series of Mathematica commands to attain the simulation results. The initial configurations of the proposed system have to be defined in the sequence of commands to be executed as shown in Table 1.

9.1 Scenario 1

Real-life tasks that must be performed expeditiously and collaboratively in dynamic construction settings, such as material handling, maintenance, welding and cleaning, are essentially the end-effector targets. In this scenario, the multi-agent system consists of five car-like mobile manipulators ($i,j \in \{1,2,3,4,5\}$) initially positioned at different locations around the workspace comprising five fixed obstacles ($q \in \{1,2,3,4,5\}$) as shown in Fig. 4(a). Each four-arm car-like manipulator is assigned a pseudo-target from which it can access four targets that represent four tasks its end-effectors must perform. Table 2 provides the numerical values of initial configurations, control, avoidance and convergence variables used in this scenario. The coordinates of the obstacles, pseudo-targets and end-effector targets are shown in Fig. 4(a), which also indicates the multi-agent system's navigation from the initial positions to the final configurations. As illustrated in Figs. 4(a) and 4(b), the initial position of the i^{th} car-like manipulator is labelled as Car i IP, while the pseudo-target and end-effector targets are labelled as Car i Targets. Fig. 4(b) shows the trajectories of the five car-like bases and their end-effectors, and the results imply that the control laws were implemented to generate feasible trajectories. Fig. 4(c) shows the profile of the Lyapunov function, $\pounds$, with its time derivative along the

Table 1: Initial configurations and parameters.

Dimensions	
Equal-sized car-like vehicles	$L \times W$
Safety parameters	ϵ_1, ϵ_2
Length of revolute links	r_{inm}
Initial Configurations	
Number of mobile manipulators	k
Position of each mobile manipulator	$(x_{c_{io}}, y_{c_{io}})$
Orientation of each mobile manipulator	$\phi_{c_{io}}$
Revolute links' angular orientations	ϕ_{inm_o}
Maximum Values	
Linear velocity of each car-like vehicle	$v_{i_{max}}$
Angular velocity of each car-like vehicle	$\omega_{i_{max}}$
Angular orientation of the 2^{nd} links of each arm	$\phi_{in2_{max}}$
Angular velocity of revolute links	$\omega_{inm_{max}}$
Restriction Parameters	
Linear velocity	ϱ_i
Angular velocity	λ_i
Revolute link angular orientation	β_{in}
Revolute link angular velocity	ρ_{in}
Control Parameters	
Each car-like vehicle's linear velocity convergence	η_{i1}
Each car-like vehicle's angular velocity convergence	η_{i2}
Revolute link angular velocity convergence	$\eta_{i_{n+2}}$
Obstacle avoidance	γ_{iq}
Moving obstacle avoidance	ξ_{ij}
Obstacles and Targets	
Number of obstacles	h
Pseudo-targets	(a_{ci}, b_{ci})

system's trajectory. The spike-free and continuous evolution of $\mathcal{L}$ shows that the trajectories are collision-free. The evolution of each car-like vehicle's angular orientation with respect to the z_1 axis is shown in Fig. 4(d). As the mobile manipulators approach their pseudo-targets, their linear and angular velocities gradually decrease to zero, as shown in Figs. 4(e) and 4(f). The decrease in velocity graphs demonstrates that the car-like vehicles are slowing down to manoeuvre around an obstacle to avoid a collision safely. The vehicles must constantly adjust their speed to adapt to the moving obstacles, which results in more frequent slowing and acceleration. Once past the obstacle, the velocity increases towards its velocity values prior to avoidance, showing a fluctuation.

The nature of the evolution of the orientation angles and angular velocities of all eight revolute links, which are of equal length, is identical for each mobile manipulator in the multi-agent system. As a result, we have only generated the graphs of angular orientations and velocities to illustrate the results for the revolute links of Car 1. The evolution of the orientation angles of the revolute links of Car 1 is shown in Fig. 5(a). Finally, the angular velocities of all the revolute links along the trajectory are illustrated in Fig. 5(b), which tend to zero as the four end-effectors approach their designated targets.

Table 2: Numerical values of parameters used in Scenario 1.

Dimensions	
$L \times W$	7×7
ϵ_1, ϵ_2	1
r_{inm}	3
Initial Configurations	
k	5
$(x_{c_{i0}}, y_{c_{i0}})$	$(x_{c_{10}}, y_{c_{10}}) = (10,8), (x_{c_{20}}, y_{c_{20}}) = (10,140), (x_{c_{30}}, y_{c_{30}}) = (140,35), (x_{c_{40}}, y_{c_{40}}) = (65,140), (x_{c_{50}}, y_{c_{50}}) = (140,70)$
$\phi_{c_{i0}}$	$\phi_{c_{10}} = \frac{\pi}{2}, \phi_{c_{20}} = 0, \phi_{c_{30}} = \phi_{c_{40}} = \phi_{c_{50}} = \pi$
ϕ_{inm_0}	$\phi_{i11_0} = \frac{150\pi}{180}, \phi_{i12_0} = \phi_{i32_0} = \frac{-148\pi}{180}, \phi_{i21_0} = \frac{-150\pi}{180}, \phi_{i122_0} = \phi_{i42_0} = \frac{148\pi}{180}, \phi_{i31_0} = \frac{-30\pi}{180}, \phi_{i41_0} = \frac{30\pi}{180},$
Maximum Values	
$v_{i_{max}}$	$v_{1_{max}} = 1, v_{2_{max}} = 3, v_{3_{max}} = 2, v_{4_{max}} = 2.5, v_{5_{max}} = 1.5$
$\omega_{i_{max}}$	2
$\phi_{in2_{max}}$	$\frac{5\pi}{6}$
$\omega_{inm_{max}}$	5
Restriction Parameters	
ϱ_i	0.01
λ_i	0.002
β_{in}	0.0002
ρ_{in}	3×10^{-6}
Control Parameters	
η_{i1}	900
η_{i2}	600
$\eta_{i_{n+2}}$	10
γ_{iq}	0.1
ξ_{ij}	0.0005
Obstacles and Targets	
h	5
(a_{ci}, b_{ci})	$(a_{c1}, b_{c1}) = (140,140), (a_{c2}, b_{c2}) = (140,13), (a_{c3}, b_{c3}) = (10,113), (a_{c4}, b_{c4}) = (10,60), (a_{c5}, b_{c5}) = (60,15)$

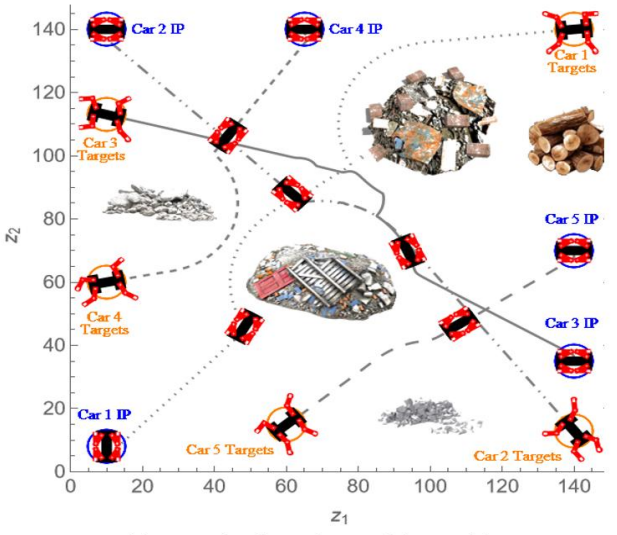

(a) Positions and orientations of the multi-agent system

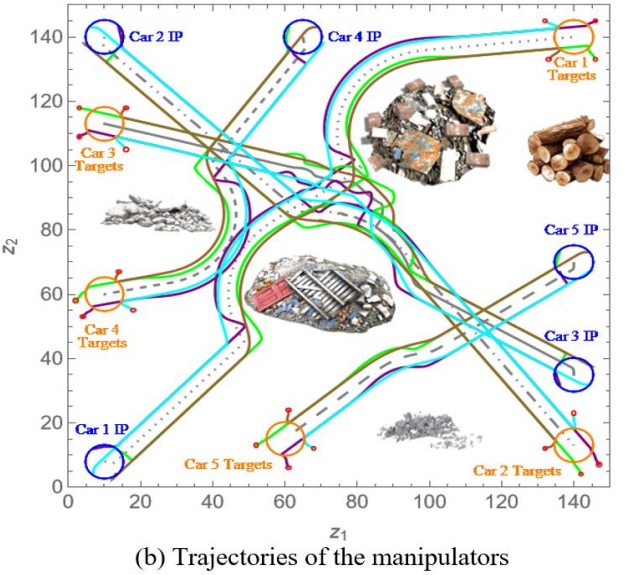

(b) Trajectories of the manipulators

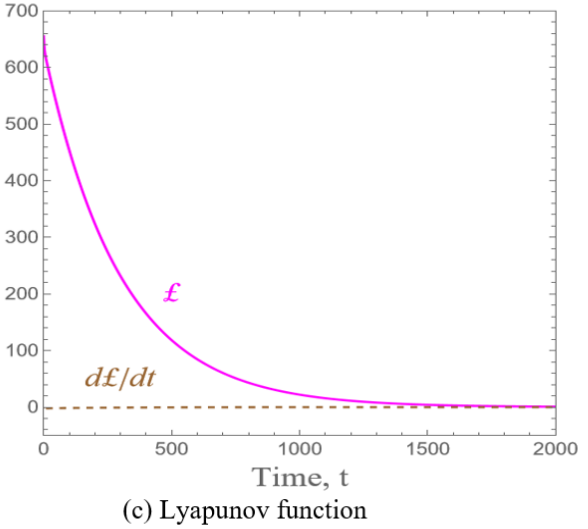

(c) Lyapunov function

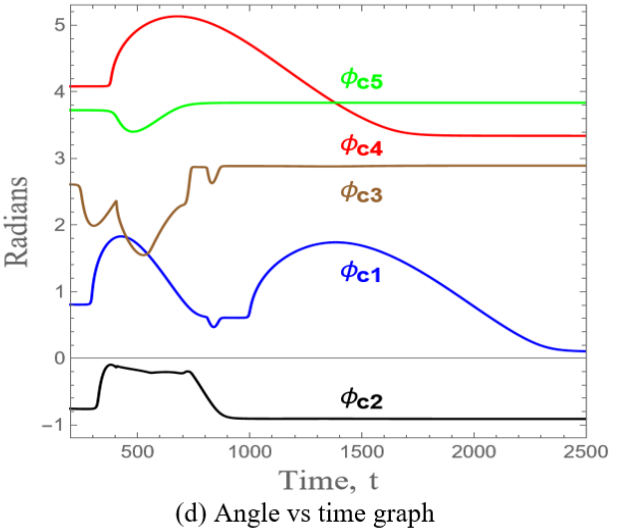

(d) Angle vs time graph

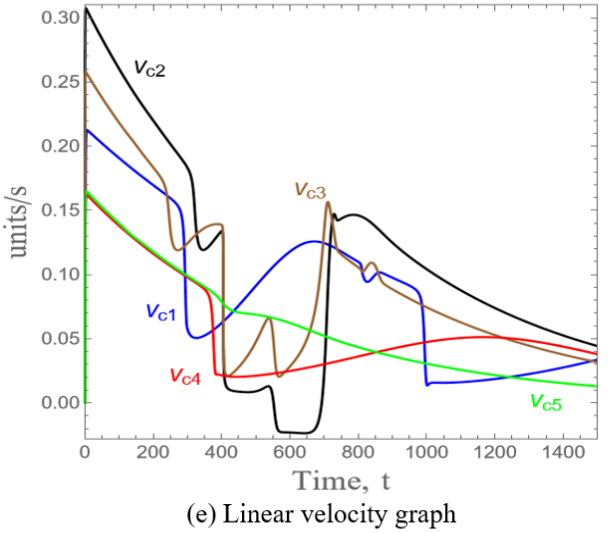

(e) Linear velocity graph

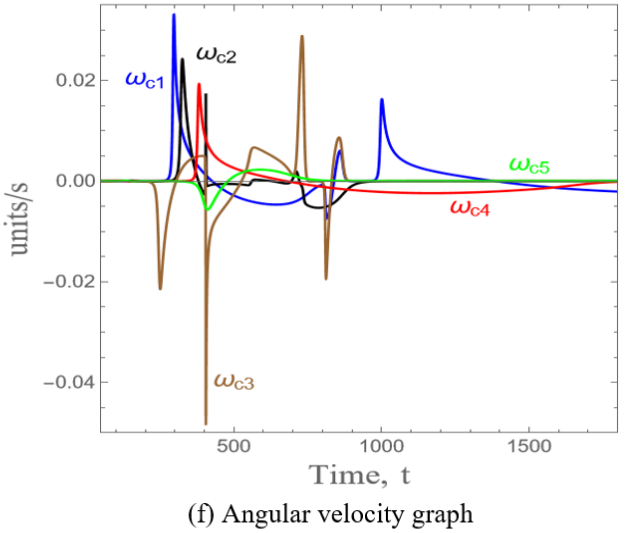

(f) Angular velocity graph

Fig. 4: (a) The multi-agent system's positions at times t = 1,300, and 40000 along its trajectories. (b) Each car-like vehicle's trajectories are traced in gray, while those of arms 1, 2, 3, and 4 are traced in purple, green, brown, and cyan, respectively. (c) Monotonically decreasing Lyapunov function with its time derivative. (d) Orientations of the five car-like vehicles. (e) Linear velocities of the car-like mobile manipulators (f) Angular velocities of the car-like mobile bases.

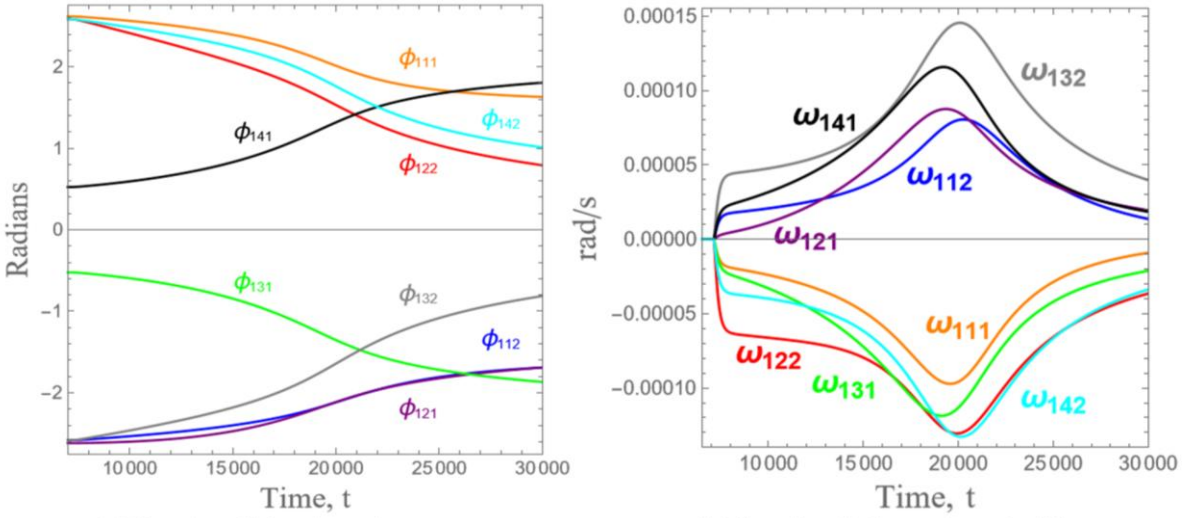

(a) Revolute link orientations (b) Revolute link angular velocities

Fig. 5: (a) Orientations of Car 1's revolute links abiding the angular restrictions and limitations. (b) Angular velocities of Car 1's revolute links.

9.2 Scenario 2

This scenario illustrates the effectiveness of the proposed control laws in enabling a team of four car-like manipulators ($i,j \in \{1,2,3,4\}$) initially parked adjacent to each other, to perform assigned tasks at the opposite end of a workspace cluttered with six fixed obstacles ($q \in \{1,2,...,6\}$). In contrast to the first two vehicles whose targets are directly opposite, the third and fourth vehicles' targets are positioned at offset locations. This implies that in addition to avoiding the fixed obstacles, Car 3 and Car 4 have to avoid each other on the way to their targets. The multi-agent system's convergence to the targets is demonstrated in Fig. 6. Table 3 provides the initial conditions and parameters utilized if different from Scenario 1. The motion and orientations of the mobile manipulators are shown in Fig. 7(a) while their trajectories are illustrated in Fig. 7(b). The behaviour of the linear velocities and the evolution of the angular velocities of the four car-like vehicles abiding by the velocity limitations and restrictions are demonstrated in Figs. 7(c) and 7(d), respectively. The fluctuations in the form of sudden increases and decreases in values noticed in the velocity graphs indicate the system's adherence to collision avoidance. The profile of the Lyapunov function, each mobile base's angular orientation and the arms' angular orientations and angular velocities are similar to that of Scenario 1.

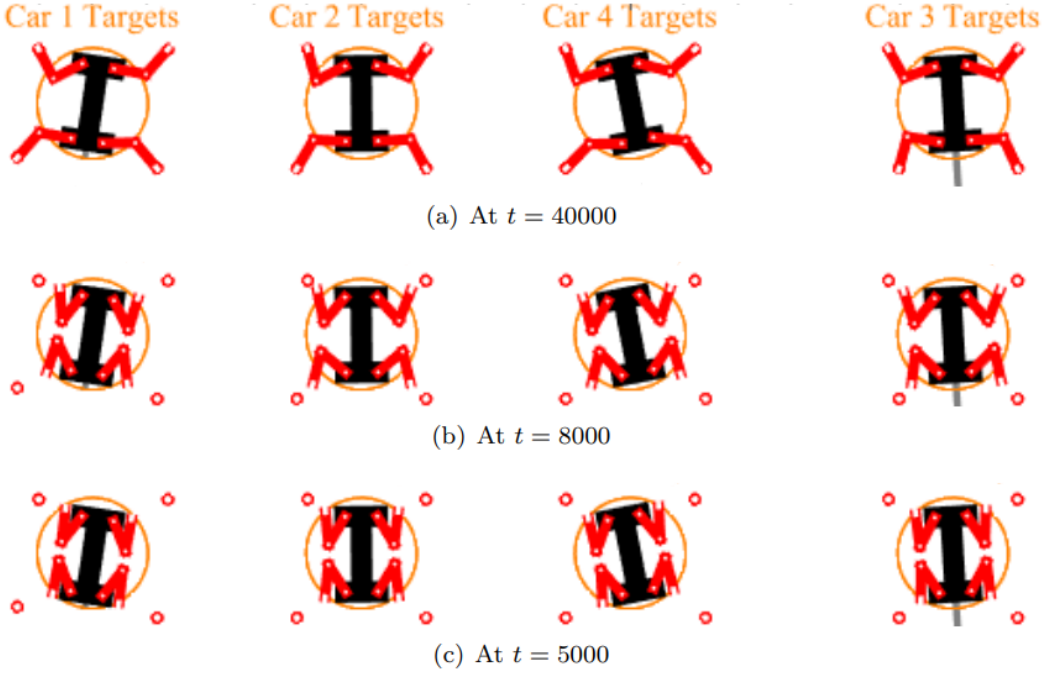

(a) At $t = 40000$

(b) At $t = 8000$

(c) At $t = 5000$

Fig. 6: Snapshots showing the convergence of the multi-agent system to the assigned targets. The acceleration-based controllers ensure that each manipulator adheres to the dual-step motion outlined in Algorithm 1. (a) The multi-agent system at its final configuration, (b) The multi-agent system's position at t =8000, and (c) The multi-agent system's position at t =5000.

Table 3: Numerical values of parameters used in Scenario 2.

Initial Configurations	
k	4
$(x_{c_{i0}}, y_{c_{i0}})$	$(x_{c_{10}}, y_{c_{10}}) = (10,10), (x_{c_{20}}, y_{c_{20}}) = (25,10),$ $(x_{c_{30}}, y_{c_{30}}) = (40,10), (x_{c_{40}}, y_{c_{40}}) = (55,10)$
$\phi_{c_{i0}}$	$\frac{\pi}{2}$
Maximum Values	
$v_{i_{max}}$	2
Obstacles and Targets	
h	6
(a_{ci}, b_{ci})	$(a_{c1}, b_{c1}) = (10,90), (a_{c2}, b_{c2}) = (35,90),$ $(a_{c3}, b_{c3}) = (60,90), (a_{c4}, b_{c4}) = (90,90)$

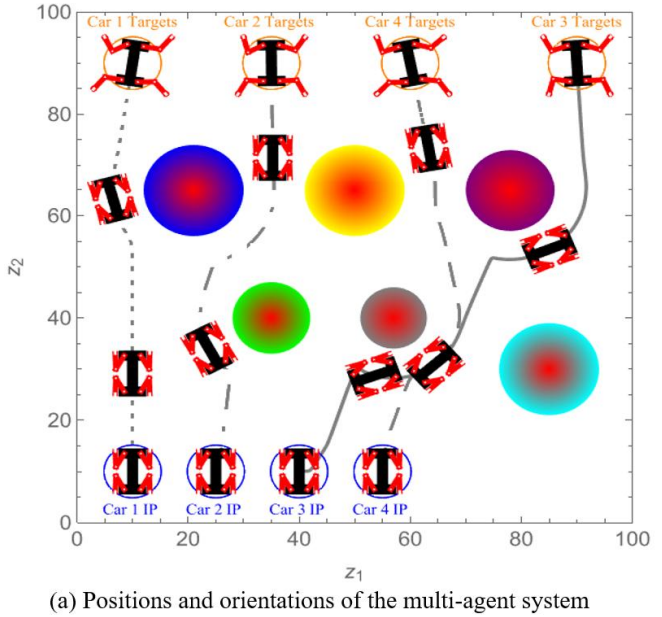

(a) Positions and orientations of the multi-agent system

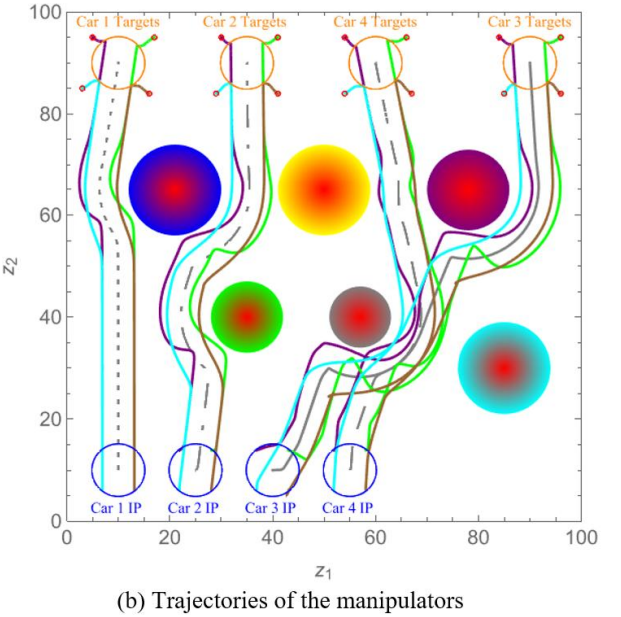

(b) Trajectories of the manipulators

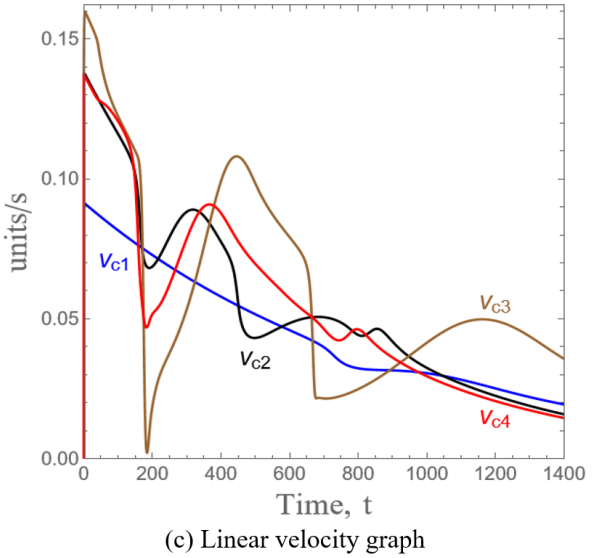

(c) Linear velocity graph

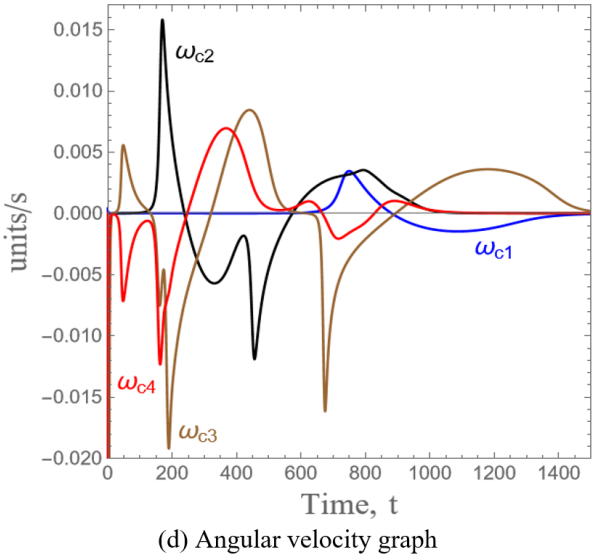

(d) Angular velocity graph

Fig. 7: (a) The multi-agent system's positions at times t =1, 240, 1000, and 40000 along its trajectories. (b) The car-like vehicles' trajectories are traced in the same colors. (c) Linear velocities of the car-like mobile manipulators. (d) Angular velocities of the car-like mobile bases.

9.3 Scenario 3

This scenario considers a multi-agent system of two mobile manipulators being subjected to perform tasks in an environment comprising two randomly generated obstacles of different sizes ($i,j,q \in \{1,2\}$). The initial position, motion, and orientations of revolute arms are illustrated in Fig. 8(a), while the trajectories of the two-car system as they maneuver to their targets are shown in Fig. 8(b). The linear and angular velocities of the vehicles are illustrated in Figs. 8(c) and (d). The profile of the Lyapunov function, each car-like mobile base's angular orientation and the revolute links angular orientations and angular velocities are similar to that of Scenario 1. The efficiency of the control laws is demonstrated in this scenario whereby the autonomous vehicles successfully avoid collisions with the fixed and moving obstacles, as depicted in Fig. 9, and clearly converge to their assigned targets. Only those parameters different from the ones given in the previous scenarios are provided in Table 4.

The acceleration-based motion controllers designed in Eqs. (38)-(40) ensure that both manipulators successfully avoid collisions amongst themselves while crossing each other's paths. In adherence to the velocity restrictions tagged to the multi-agent system, Car 1 slows down to allow Car 2 to pass through before proceeding. This result is clearly illustrated in the velocity graphs obtained in Figs. 8(c) and 8(d). The trajectory colours are the same as stated in Fig. 4(b), and both manipulators' paths are the same as shown in Fig. 8(a). The orientation and position of both vehicles at $t = 300, 400, 450, 500, 600$ and 850, respectively, show that both vehicles can achieve collision-free trajectories as desired.

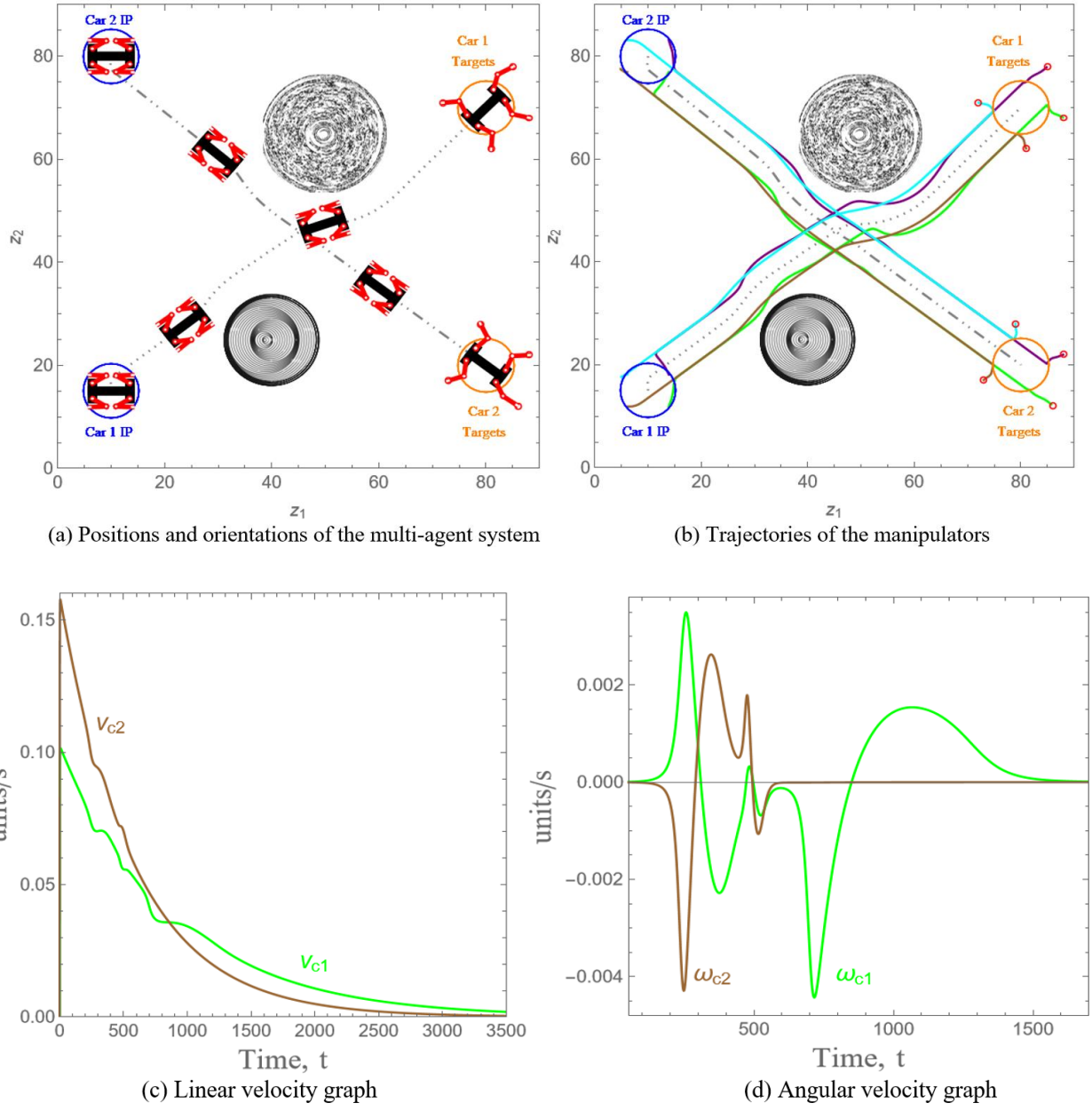

(a) Positions and orientations of the multi-agent system

(b) Trajectories of the manipulators

(c) Linear velocity graph

(d) Angular velocity graph

Fig. 8: (a) The multi-agent system's positions at times t = 1,200,750 and 40000. (b) The car-like vehicles' trajectories are traced in the same colors. (c) Linear velocities of the car-like mobile manipulators. (d) Angular velocities of the car-like mobile bases.

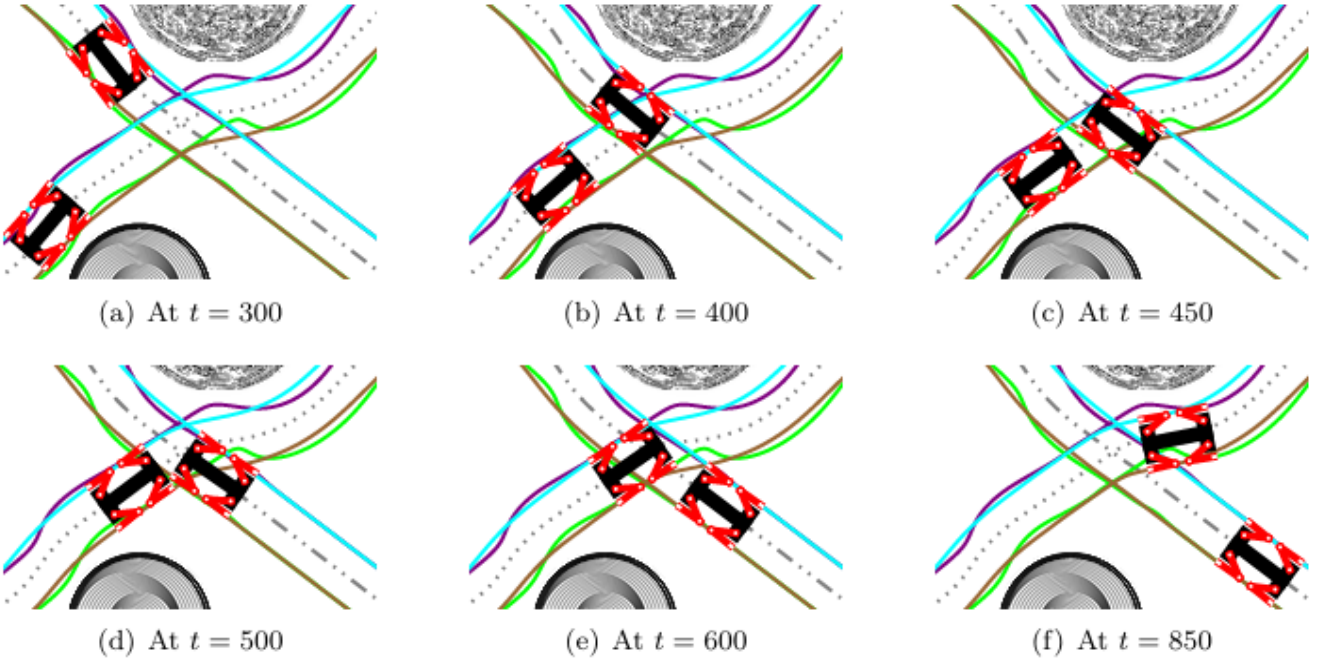

Fig. 9: Snapshots showing the two car-like vehicles approaching and avoiding collision with each other on their way to their targets. (a) The two mobile manipulators approaching each other, (b) Car 1 slows down to allow Car 2 to pass, (c) Car 2 passes by at t =450, (d) Positions of the two cars at t =500, (e) Successful collision avoidance, and (f) The mobile manipulators continue along their trajectories.

The acceleration-based motion controllers designed in Eqs. (38)-(40) ensure that both manipulators successfully avoid collisions amongst themselves while crossing each other's paths. In adherence to the velocity restrictions tagged to the multi-agent system, Car 1 slows down to allow Car 2 to pass through before proceeding. This result is clearly illustrated in the velocity graphs obtained in Figs. 8(c) and 8(d). The trajectory colours are the same as stated in Fig. 4(b), and both manipulators' paths are the same as shown in Fig. 8(a). The orientation and position of both vehicles at $t = 300, 400, 450, 500, 600$ and 850, respectively, show that both vehicles can achieve collision-free trajectories as desired.

9.4 Remark

The results indicate that the autonomous multi-agent system of car-like manipulators successfully implemented the dual-step algorithm and the acceleration-based controllers to accomplish multiple assigned tasks in obstacle-ridden dynamic environments. The dynamic constraints, limitations, and acceleration-based motion controllers enabled the mobile manipulators to successfully avoid collisions with fixed and moving obstacles and produce feasible collision-free trajectories. The safe and smooth trajectories in scenarios 1, 2, and 3 imply that this approach can be effectively used in real-life applications where multiple tasks are to be performed in dynamic environments.

Compared to the multi-robotic systems presented in Refs. [8], [11], and [12], the proposed multi-agent system offers enhanced scalability and task adaptability through its modular design, which integrates car-like mobile bases with four-arm manipulators on each unit. In contrast to heuristic or sampling-based planners such as those in Refs. [7] and [14], which often encounter challenges related to manipulation constraints or require intensive mode-switch optimization, the proposed method enables coordination and motion feasibility without significant computational complexity. Furthermore, the Lyapunov-based acceleration controllers developed in this study outperform the velocity-based controllers of Ref. [13], which are susceptible to erratic motion in dynamic environments. The proposed controllers generate smoother

Table 4: Numerical values of parameters used in Scenario 3.

Initial Configurations	
k	2
$(x_{c_{i0}}, y_{c_{i0}})$	$(x_{c_{10}}, y_{c_{10}}) = (10,15), (x_{c_{20}}, y_{c_{20}}) = (10,80)$
$\phi_{c_{i0}}$	0
Obstacles and Targets	
h	2
(a_{ci}, b_{ci})	$(a_{c1}, b_{c1}) = (80,70), (a_{c2}, b_{c2}) = (80,20)$

and safer trajectories, essential for reliable operation in complex construction settings. This enhances the system's ability to navigate and perform tasks efficiently, enabling seamless agent collaboration in dynamic environments. Overall, the proposed system demonstrates a higher degree of autonomy, precision and robustness than many existing state-of-the-art multi-agent robotic platforms used in construction automation.

10. Discussion

The acceleration-based motion controllers derived from LbCS have been utilized in this research to guide the multi-agent system of mobile manipulators, equipped with four robotic arms each, to their pseudo-targets and ultimate end-effector targets. The proposed technique provides solutions for performing complex and tiresome tasks through multi-agent robotic automation, with implications for enhanced operational efficiency and worker safety in dynamic environments. Apart from the controllers' effectiveness in producing smooth motion for navigation, the system's capability to execute multiple repetitious tasks as multiple agents guarantee that the proposed system can be easily implemented to autonomously perform a range of tasks in diverse environments such as construction, waste management, environmental conservation and smart cities.

As depicted by the results in Section 9, the multi-agent system can speed up processes by executing multiple tasks simultaneously that could have otherwise been performed at a slower rate by a single car-like manipulator, as shown in Ref. [6]. While Sartoretti *et al*.[12] utilized actor-critic algorithms with TERMES robots for block assembly, their system was limited to simpler tasks and had reduced manipulator degrees of freedom. In contrast, our four-arm configuration increases the system's ability to perform concurrent complex construction operations such as assembling, lifting, and transporting components. For situations requiring faster project completion and reducing labour costs, the multi-robot system proposed in this research is a better, more comprehensive and cost-effective option than the two cooperative dual-arm manipulators utilized in Ref. [11] or the collaborative robots used in Ref. [24]. Such homogeneous systems can easily adapt to changing project requirements by reallocating tasks among agents, making them suitable for small and large projects across diverse sectors. Furthermore, for specific tasks such as material handling and complex assembly operations that require extensive labour, the proposed team of mobile manipulators can execute such tasks with ease, as demonstrated in Figs. 4(a), 7(a) and 8(a).

Multi-agent systems of four-arm car-like mobile manipulators hold great potential in carrying out multiple tasks and speeding up project timelines without compromising quality and work standards in dynamic construction environments. Therefore, it is feasible to include the approach presented in this research in specific applications that require material handling tasks and complex assembly processes to be performed quickly, effectively and efficiently.

11. Conclusion

Issues such as labour shortages, worker safety and project delays, which are continuously faced by the construction industry, can be addressed by integrating advanced robotics technologies. The multi-agent system of mobile manipulators presented in this research offers innovative solutions to these challenges by automating labour-intensive tasks, improving safety and increasing productivity. The development of continuous acceleration-based controllers for the multi-agent system represents a significant advancement in autonomous construction operations. These motion controllers, designed using LbCS, enhance the proposed multi-agent system's performance and manoeuvrability in dynamic environments. The system's collision-free navigation has been assessed through computer simulations, implying that this system can perform complex tasks with increased efficiency and flexibility. To the best of the authors' knowledge, this is the first time such continuous, stabilizing and non-linear acceleration-based motion controllers are designed using LbCS to solve the motion planning and control problem of a multi-agent system of four-arm car-like mobile manipulators.

Nonetheless, further research is needed to fully harness the potential of a network of multiple four-arm car-like mobile manipulators to perform construction tasks in evolving dynamic environments such as smart cities. For effective operations in constrained and obstacle-cluttered environments, future work will include analysis of the multi-agent system's work efficiency, using the minimum distance technique for obstacle avoidance and flushing off the drawback of workspace being wasted due to enclosing each mobile manipulator in a circular protective region. This approach will enable the mobile manipulators to manoeuvre safely in constrained, narrow spaces amongst different dynamic obstacles.

Conflict of Interest

There is no conflict of interest.

Supporting Information

Not applicable.

References

[1] Z. Huang, C. Mao, J. Wang, A. M. Sadick, Understanding the key takeaway of construction robots towards construction automation, *Engineering, Construction and Architectural*

Management, 2022, **29**, 3664-3688, doi: 10.1108/ecam-03-2021-0267.

[2] Z. Zhou, J. Zhou, B. Zhang, J. Alcalá, V. Yepes, The centennial sustainable assessment of regional construction industry under the multidisciplinary coupling model, *Sustainable Cities and Society*, 2024, **101**, 105201, doi: 10.1016/j.scs.2024.105201.

[3] M. A. Hossain, A. Zhumabekova, S. C. Paul, J. R. Kim, A review of 3D printing in construction and its impact on the labor market, *Sustainability*, 2020, **12**, 8492, doi: 10.3390/su12208492.

[4] K. Kaya, Planning the future of smart cities with swarms of fully autonomous unmanned aerial vehicles using a novel framework, *IEEE Access*, 2021, **9**, 6571-6595, doi: 10.1109/ACCESS.2020.3049094.

[5] M. Krizmancic, B. Arbanas, T. Petrovic, F. Petric, S. Bogdan, Cooperative aerial-ground multi-robot system for automated construction tasks, *IEEE Robotics and Automation Letters*, 2020, **5**, 798-805, doi: 10.1109/LRA.2020.2965855.

[6] A. Prasad, B. Sharma, J. Vanualailai, S. Kumar, Motion control of an articulated mobile manipulator in 3D using the Lyapunov-based control scheme, *International Journal of Control*, 2022, **95**, 2581-2595, doi: 10.1080/00207179.2021.1919927.

[7] V. N. Hartmann, A. Orthey, D. Driess, O. S. Oguz, M. Toussaint, Long-horizon multi-robot rearrangement planning for construction assembly, *IEEE Transactions on Robotics*, 2023, **39**, 239-252, doi: 10.1109/TRO.2022.3198020.

[8] F. Kennel-Maushart, R. Poranne, S. Coros, Interacting with multi-robot systems *via* mixed reality, *2023 IEEE International Conference on Robotics and Automation (ICRA)*, May 29-June 2, London, United Kingdom, IEEE, 2023, 11633-11639, doi: 10.1109/ICRA48891.2023.10161412.

[9] Y. Zhou, J. Luo, M. Wang, Dynamic manipulability analysis of multi-arm space robot, *Robotica*, 2021, **39**, 23-41, doi: 10.1017/s0263574720000077.

[10] W. Amanhoud, J. Hernandez Sanchez, M. Bouri, A. Billard, Contact-initiated shared control strategies for four-arm supernumerary manipulation with foot interfaces, *The International Journal of Robotics Research*, 2021, **40**, 986-1014, doi: 10.1177/02783649211017642.

[11] D. Sanchez, W. Wan, K. Harada, Four-arm collaboration: two dual-arm robots work together to manipulate tethered tools, *IEEE/ASME Transactions on Mechatronics*, 2022, **27**, 3286-3296, doi: 10.1109/TMECH.2021.3106644.

[12] G. Sartoretti, Y. Wu, W. Paivine, T. K. Satish Kumar, S. Koenig, H. Choset, Distributed reinforcement learning for multi-robot decentralized collective construction, *Distributed Autonomous Robotic Systems*, Cham: Springer International Publishing, 2019, 35-49, doi: 10.1007/978-3-030-05816-6_3.

[13] J. Vanualailai, B. Sharma, S. I. Nakagiri, An asymptotically stable collision-avoidance system, *International Journal of Non-Linear Mechanics*, 2008, **43**, 925-932, doi: 10.1016/j.ijnonlinmec.2008.06.012.

[14] D. Wallace, Y. H. He, J. Chagas Vaz, L. Georgescu, P. Y. Oh, Multimodal Teleoperation of Heterogeneous Robots within a Construction Environment, *2020 IEEE/RSJ International Conference on Intelligent Robots and Systems (IROS)*, October 24, 2020-January 24, 2021, Las Vegas, NV, USA, IEEE, 2020, doi: 10.1109/iros45743.2020.9340688.

[15] A. Akinsemoyin, I. Awolusi, D. Chakraborty, A. J. Al-Bayati, A. Akanmu, Unmanned aerial systems and deep learning for safety and health activity monitoring on construction sites, *Sensors*, 2023, **23**, 6690, doi: 10.3390/s23156690.

[16] Y. Miron, D. Navon, Y. Goldfracht, D. Di Castro, I. Klein, Decentralized and asymmetric multi-agent learning in construction sites, *IEEE Open Journal of Vehicular Technology*, 2024, **5**, 1587-1599, doi: 10.1109/OJVT.2024.3479927.

[17] X. Li, J. Ren, Y. Li, Multi-mode filter target tracking method for mobile robot using multi-agent reinforcement learning, *Engineering Applications of Artificial Intelligence*, 2024, **127**, 107398, doi: 10.1016/j.engappai.2023.107398.

[18] K. Chaudhary, V. Chand, A. Prasad, B. Sharma, Robot motion control using dual avoidance scheme, *Engineered Science*, 2024, **32**, 1261, doi: 10.30919/es1261.

[19] K. Chaudhary, A. Prasad, V. Chand, B. Sharma, ACO-Kinematic: a hybrid first off the starting block, *PeerJ Computer Science*, 2022, **8**, e905, doi: 10.7717/peerj-cs.905.

[20] T. Hosmer, S. Mutis, O. Gheorghiu, P. Siedler, Z. He, B. Erdincer, Autonomous ecologies of construction: Collaborative modular robotic material eco-systems with deep multi-agent reinforcement learning, *International Journal of Architectural Computing*, 2024, **22**, 661-688, doi: 10.1177/14780771241287827.

[21] S. A. Kumar, R. P. Chand, R. Chand, B. Sharma, Entertainment and assistive robot: acceleration controllers of an autonomous kids personal transporter (kPT), *Engineered Science*, 2024, **32**, 1318, doi: 10.30919/es1318.

[22] C. Cohen, D. Rouhling, A formal proof in coq of LaSalle's invariance principle, *Interactive Theorem Proving*, Cham: Springer International Publishing, 2017, 148-163, doi: 10.1007/978-3-319-66107-0_10.

[23] J. LaSalle, Some extensions of liapunov's second method, *IRE Transactions on Circuit Theory*, 1960, **7**, 520-527, doi: 10.1109/TCT.1960.1086720.

[24] H. Eberle, S. J. Nasuto, Y. Hayashi, Synchronization-based control for a collaborative robot, *Royal Society Open Science*, 2020, **7**, 201267, doi: 10.1098/rsos.201267.

Publisher's Note: Engineered Science Publisher remains neutral with regard to jurisdictional claims in published maps and institutional affiliations.

Open Access
This article is licensed under a Creative Commons Attribution 4.0 International License, which permits the use, sharing, adaptation, distribution and reproduction in any medium or format, as long as appropriate credit to the original author(s) and the source is given by providing a link to the Creative Commons license and changes need to be indicated if there are any. The images or other third-party material in this article are included in the article's Creative Commons license, unless indicated otherwise in a credit line to the material. If material is not included in the article's Creative Commons license and your intended use is not permitted by statutory regulation or exceeds the permitted use, you will need to obtain permission directly from the copyright holder. To view a copy of this license, visit http://creativecommons.org/ licenses/by/4.0/.

©The Author(s) 2025